8-26-86
R.C.

NASA-CR-174894

R85-956834

ASSESSMENT OF A 3-D BOUNDARY LAYER ANALYSIS TO PREDICT HEAT TRANSFER AND FLOW FIELD IN A TURBINE PASSAGE

R-G
3-17-86

by

O.L. Anderson

Prepared for:

National Aeronautics and Space Administration
Lewis Research Center

NASA Contract NAS3-23716

UNITED TECHNOLOGIES RESEARCH CENTER
East Hartford, Connecticut 06108

R85-956834

Assessment of a 3-D Boundary Layer Analysis to Predict Heat Transfer and Flow Field in a Turbine Passage

TABLE OF CONTENTS

R85-956834

Assessment of a 3-D Boundary Layer Analysis to Predict Heat Transfer and Flow Field in a Turbine Passage

1.0 SUMMARY

An assessment has been made of the applicability of a three dimensional boundary layer analysis to the calculation of heat transfer, total pressure losses, and streamline flow patterns on the surfaces of both stationary and rotating turbine passages. In support of this effort, an analysis has been developed to calculate a general nonorthogonal surface coordinate system for arbitrary three dimensional surfaces and also to calculate the boundary layer edge conditions for compressible flow using the surface Euler equations and experimental pressure distributions. Using available experimental data to calibrate the method, calculations are presented for the pressure, endwall, and suction surfaces of a stationary cascade and for the pressure surface of a rotating turbine blade. The results strongly indicate that the three dimensional boundary layer analysis can give good predictions of the flow field, loss, and heat transfer on the pressure, suction, and endwall surface of a gas turbine passage.

2.0 INTRODUCTION

The prediction of the complete flow field in a turbine passage is an extremely difficult task due to the complex three-dimensional flow pattern which contains separation and attachment lines, a saddle point, and a horseshoe vortex (Fig. 1). Whereas, in principal such a problem can be solved using full Navier-Stokes equations, in reality methods based on a Navier-Stokes solution procedure encounter difficulty in accurately predicting surface quantities, such as heat transfer, due to grid limitations imposed by the speed and size of the existing computers. On the other hand the overall problem is strongly three dimensional and too complex to be analyzed by the current design methods based on inviscid and/or viscous strip theories. Thus there is a strong need for local enhancing of the current prediction techniques through inclusion of 3-D viscous effects. A potentially simple and cost effective way to achieve this goal is to use a prediction method based on three dimensional boundary layer (3-DBL) theory. The major objective of this study is to assess the applicability of such a 3-DBL approach for the prediction of heat loads, boundary layer growth, pressure losses, and streamline skewing in critical areas of a turbine passage. For this purpose, the three dimensional boundary layer analysis developed by Vatsa (Ref. 1 and 2) has been selected to evaluate this approach as a means for calculating the local properties of the flow field.

In this approach zonal concepts are utilized to delineate regions of application of 3-DBL theory - these being the endwall surface, suction surface, and pressure surface of a turbine blade as shown by the shaded regions of Fig. 1. The zonal concept employed in this study implies that there exists a thin region near the surface dominated by wall pressure forces, friction forces, and Coriolis forces so that boundary layer theory is valid provided that the proper inflow conditions and boundary layer edge conditions are specified. Although the pressure surface of a stationary blade (cascade) shows only weak three dimensional effects, the suction surface shows strong effects due the nearby passage vortex which sweeps the flow from the endwall. Likewise the pressure surface of a rotating turbine blade shows strong three dimensional effects due to the interaction of the strong radial pressure gradient and the Coriolis force. These strong three dimensional effects should provide a rigorous test of the zonal application of 3-D boundary layer theory to the turbine.

This zonal approach requires three separate analyses: 1) an analysis to construct a general non-orthogonal surface coordinate system for twisted turbine blades, 2) an analysis to calculate the boundary layer edge conditions from a known static pressure distribution, and 3) a 3-D boundary layer analysis which predicts the boundary layer growth with prescribed inflow conditions. A review of the background literature on these three problems is given below.

A coordinate system must have certain general properties if it is to be useful for calculating three dimensional boundary layer solutions. Since the

boundary layers lie on the turbine blade surface, a useful coordinate system would be one formed by the intersection of three sets one parameter surfaces of which two sets of surfaces intersect the wall boundary and the third set of surfaces move off the wall boundary in a one parameter set. In such a coordinate system, one surface of the third set is the boundary surface which is described by only two parameters (coordinates). Thus as an example Howarth (Ref. 3) derived the three dimensional boundary layer equations in a general orthogonal coordinate system which fits this requirement. However triply orthogonal coordinate systems are difficult to construct for arbitrary surfaces such as a twisted turbine blade. Squire (Ref. 4) derived a more general set of of boundary layer equations in a restricted nonorthogonal coordinate system. However this set of equations has certain coordinate curvature restrictions which make it difficult to apply in practical cases. If, however, one makes the assumption that the boundary layers are very thin compared to the radius of curvature of the surface, then the problem is greatly simplified. In this situation the third set of surfaces is approximated by the boundary surface and is called a surface coordinate system. In this surface coordinate system, two coordinates lie on the surface and the third is normal to the surface. In addition it should be noted that on the boundary surface, it is difficult to construct two orthogonal families of curves to describe the surface. Thus it is desirable to have a nonorthogonal coordinate system on the surface. The problem then reduces to the mapping of the three dimensional boundary surface to a plane surface to be described by two one parameter families of curves (coordinates). This mapping function has been developed by Gordon and Thiel (Ref. 5) and the construction of a general nonorthogonal surface coordinate system for arbitrary surfaces is described in this report. Since turbine blades are rotating, another requirement of the coordinate system is that it should be a rotating coordinate sysem so that the Coriolis, or apparent forces, appear explicity in the boundary layer equations. Mager (Ref. 6) has derived the boundary layer equations in a general orthogonal rotating coordinate system. However, as stated earlier, a nonorthogonal surface coordinate system is more useful. Vatsa (Ref. 1 and 2) has derived a set of boundary layer equations in a nonorthogonal rotating surface coordinate system which meets all these requirements and therefore this analysis has been used to make the assessment presented in this study.

The solution of the boundary layer equations requires specification of the boundary layer edge conditions. These conditions are the two components of the edge velocity, the edge total enthalpy (rothalpy), and the thermodynamic variables of state. These edge conditions can be obtained directly from experimental data or they can be obtained from solutions of the Euler equations. Measurements of the vector velocity components in a three dimensional flow field are extremely difficult and costly to obtain. Difficulties are also encountered in the use of the Euler equations for the boundary layer edge conditions since these solutions do not produce secondary flows which are generated by viscous shear forces. An alternative approach is to obtain the edge conditions by solving the Euler

equations evaluated at the surface (hereafter referred to as surface Euler equations) using a known (experimental) pressure distribution. This approach fits well within the scope of the present program since the overall objective is the assessment of 3DBL analysis for turbine flows. Since static pressure distributions over surface are relatively easy to obtain, this method is more straightforward and avoids the problems mentioned above. This method was outlined by Cebeci (Ref. 7) for application to aircraft wings. Gleyzes and Cousteix (Ref. 8) developed a similar method for incompressible flow over fusiform bodies. This report extends this method to the prediction of the boundary layer edge velocities and thermodynamic quantities for compressible flow over general three dimensional surfaces.

A detailed review of the development of three dimensional boundary layer theory is given by Vatsa (Refs. 1 and 2). In this report only a brief outline of the methods used by Vatsa shall be given. It has long been recognized that turbulent boundary layer growth is governed by two length scales that have different properties. Near the wall the turbulence is affected by the presence of the wall and the inner length scale reflects this property of the turbulence. Thus flow is described by the well known law of the wall. Far from the wall, the turbulence is wakelike in behavior and an outer layer length scale describes the turbulence properties. For two dimensional laminar boundary layers, the Levy-Lees transformation, such as that used by Blottner (Ref. 9), attempts to capture the growth of the boundary layer and thereby significantly simplifying the analysis. For turbulent boundary layers, Werle and Verdon (Ref. 10) have generalized this concept by replacing the molecular edge viscosity with an effective turbulent viscosity. Vatsa (Ref. 1 and 2) has generalized these concepts to three dimensional turbulent boundary layers and has sucessfully obtained solutions to a number of problems.

In this report, an assessment of the applicability of a three dimensional boundary layer analysis to the calculation of heat transfer, total pressure loss, and streamline skewing on turbine blades is made using the 3-D boundary layer analysis of Vatsa (Refs. 1 and 2). In support of this assessment an analysis has been developed to construct a general nonorthogonal surface coordinate system for arbitrary three dimensional surfaces and an analysis has also been developed to calculate the boundary layer edge conditions using the surface Euler equations and experimental surface static pressure distributions. Both of these analyses are explained in detail in Section 3 - Analysis, along with a review of the 3DBL analysis developed by Vatsa. In Section 4 - Results and Discussion, available experimental data is used to calibrate the method with calculations presented for the pressure, endwall, and suction surface of a gas turbine cascade described by Graziani et. al. (Ref. 11) and for the the pressure surface of a rotating turbine blade described by Dring and Joslyn (Refs. 12 and 13).

3.0 ANALYSIS

3.1 Surface Coordinate System

The three dimensional boundary layer equations are written in a surface coordinate system (x_1, x_2, x_3) in which x_1 and x_2 lie on the surface and x_3 is orthogonal to (x_1, x_2) and hence normal to the surface. The coordinate x_1 is generally in the streamwise direction and x_2 is generally in the crossflow direction. If the coordinates of the surface are written in Cartesian coordinates (y_1, y_2, y_3), and the transformation

$$y_i = y_i\,(x_j) \tag{3.1.1}$$

is known, where the Jacobian

$$J = \left|\frac{\partial y_i}{\partial x_j}\right| \neq 0 \tag{3.1.2}$$

then the components of the covariant metric tensor are given by Warsi (Ref. 14)

$$g_{ij} = \frac{\partial y_k}{\partial x_i}\,\frac{\partial y_k}{\partial x_j} \tag{3.1.3}$$

For the surface coordinates defined above, Eq. (3.1.3) reduces to

$$g_{11} = \left(\frac{\partial y_1}{\partial x_1}\right)^2 + \left(\frac{\partial y_2}{\partial x_1}\right)^2 + \left(\frac{\partial y_3}{\partial x_1}\right)^2 \tag{3.1.4}$$

$$g_{12} = \frac{\partial y_1}{\partial x_1}\,\frac{\partial y_1}{\partial x_2} + \frac{\partial y_2}{\partial x_1}\,\frac{\partial y_2}{\partial x_2} + \frac{\partial y_3}{\partial x_1}\,\frac{\partial y_3}{\partial x_2} \tag{3.1.5}$$

$$g_{13} = 0 \tag{3.1.6}$$

$$g_{21} = g_{12} \tag{3.1.7}$$

$$g_{22} = \left(\frac{\partial y_1}{\partial x_2}\right)^2 + \left(\frac{\partial y_2}{\partial x_2}\right)^2 + \left(\frac{\partial y_3}{\partial x_2}\right)^2 \tag{3.1.8}$$

$$g_{23} = 0 \tag{3.1.9}$$

$$g_{31} = 0 \tag{3.1.10}$$

$$g_{32} = 0 \tag{3.1.11}$$

$$g_{33} = 1 \tag{3.1.12}$$

The determant of the metric tensor is given by

$$|g| = g_{11}g_{22} - g_{12}^2 \tag{3.1.13}$$

and the metric scale coefficients are

$$h_1 = \sqrt{g_{11}} \tag{3.1.14}$$

$$h_2 = \sqrt{g_{22}} \tag{3.1.15}$$

$$h_3 = 1 \tag{3.1.16}$$

Arc lengths along the coordinates are then determined by the relations

$$ds_1 = h_1 dx_1 \tag{3.1.17}$$

$$ds_2 = h_2 dx_2 \tag{3.1.18}$$

$$ds_3 = dx_3 \tag{3.1.19}$$

It is noted that the angle between x_1 and x_2 in nonorthogonal coordinates is given by

$$\cos\theta = g_{12}/(h_1 h_2) \tag{3.1.20}$$

The surface coordinates (x_1, x_2, x_3) are the computational coordinates. The Cartesian coordinates (y_1, y_2, y_3), which are used as a basis for the transformation, are the physical coordinates. The transformation, Eq. (3.1.1), defines a unique point in physical space with its corresponding point in computational space. In order to insure uniqueness, the Jacobian Eq. (3.1.2), must never pass through zero anywhere in the computational domain. This occurs at the leading edge and trailing edge of a turbine blade. Therefore the computational domain must extend from a point just downstream from the leading edge of the blade to a point just upstream of the trailing edge of the blade. In general (x_1, x_2, x_3) do not represent physical distances along the surface of the blade. The physical distances along the coordinates, which lie on the surface of the blade, are obtained from the metric scale coefficients using Eqs. (3.1.7 through 3.1.19). A special case of surface coordinates is orthogonal coordinates on a plain surface. For this special case we have

$$g_{11} = 1 \tag{3.1.20}$$

$$g_{12} = 0 \tag{3.1.21}$$

$$g_{22} = 1 \tag{3.1.22}$$

and, as can be seen, the physical and computational coordinates are identical. Although it is possible to construct other simple coordinate systems by analytic means, these coordinates are not useful for turbine blades. Since turbine blades are twisted surfaces and their coordinates are not known except in numerical form, special analysis is required to construct a general surface coordinate system. This analysis is described in Section 3.10.

3.2 Boundary Layer Equations

An ideal set of equations for this problem consists of the three dimensional boundary layer equations in a general nonorthogonal rotating coordinate system so the Coroilis forces appear explicitly in equations. In addition to the generalized geometry required for realistic turbine blades, it is noted that boundary layers on turbine blades are laminar, transitional, and/or turbulent. Therefore the boundary layer equations should include the Reynold's stress components so that the appropriate turbulence models can be applied. Vatsa (Refs. 1 and 2) has derived a set of three dimensional turbulent boundary layer equations that meet these requirements. This derivation is long and involved and therefore will only be outlined in this section. The first step is to transform the Navier-Stokes equations from a stationary Cartesian coordinate system to a moving coordinate system using the Galilian transformation,

$$\tilde{\vec{y}} = \vec{y} + \vec{v}_B \tau \tag{3.2.1}$$

$$\tilde{\vec{u}} = \vec{u} + \vec{v}_B \tag{3.2.2}$$

$$\vec{v}_B = \vec{\Omega} \times \vec{r} \tag{3.2.3}$$

The second step is to derive the Reynolds stress terms and include them with the molecular viscous stress terms by taking an ensemble average over all possible instantaneous flow conditions,

$$\overline{f} = \lim_{N \to \infty} \frac{1}{N} \Sigma f \tag{3.2.4}$$

where f represents any combination of dependent variables. All products of the dependent variables are then separated into its average and fluctuating components (correlations).

$$\overline{fg} = \overline{f}\,\overline{g} + \overline{f'g'} \qquad (3.2.5)$$

The fluctuating components are then included with the molecular stress terms. For compressible flow, the number of terms is greatly reduced by neglecting terms with triple correlations and correlations with density fluctuations. The Navier-Stokes equations are then transformed from the Cartesian coordinate system (y_1, y_2, y_3) to a general nonorthogonal coordinate system (x_1, x_2, x_3) and then reduced to a surface coordinate system using the simplified covarient metric tensor components defined by Eqs. (3.1.4) through (3.1.12). Finally the equations are simplified using the boundary layer assumptions. Using this procedure Vatsa (Refs. 1 and 2) has derived the following set of equations using the tensor relations given by Warsi (Ref. 6).

Continuity Equation

$$\frac{\partial}{\partial x_1}\left(\frac{\sqrt{g}}{h_1}\rho u_1\right) + \frac{\partial}{\partial x_2}\left(\frac{\sqrt{g}}{h_2}\rho u_2\right) + \frac{\partial}{\partial x_3}\left(\sqrt{g}\,\rho u_3\right) = 0 \qquad (3.2.6)$$

X_1 Momentum Equation

$$\frac{u_1}{h_1}\frac{\partial u_1}{\partial x_1} + \frac{u_2}{h_2}\frac{\partial u_1}{\partial x_2} + u_3\frac{\partial u_1}{\partial x_3}$$

$$+ u_1u_1\frac{g_{12}}{g}\left\{\frac{g_{12}}{h_1^2}\frac{\partial h_1}{\partial x_1} + \frac{\partial h_1}{\partial x_2} - \frac{1}{h_1}\frac{\partial g_{12}}{\partial x_1}\right\}$$

$$+ u_1u_2\frac{1}{g}\left\{h_1h_2\left[1+\left(\frac{g_{12}}{h_1h_2}\right)^2\right]\frac{\partial h_1}{\partial x_2} - 2g_{12}\frac{\partial h_2}{\partial x_1}\right\}$$

$$+ u_2u_2\frac{h_1}{g}\left\{\frac{\partial g_{12}}{\partial x_2} - h_2\frac{\partial h_2}{\partial x_1} - \frac{g_{12}}{h_2}\frac{\partial h_2}{\partial x_2}\right\}$$

$$- 2 \frac{h_1 h_2}{\sqrt{g}} \omega_3 u_2 - 2 \frac{g_{12}}{\sqrt{g}} \omega_3 u_1$$

$$- \omega^2 r \frac{h_1 h_2^2}{g} \frac{\partial r}{\partial x_1} + \omega^2 r \frac{h_1 g_{12}}{g} \frac{\partial r}{\partial x_2}$$

$$+ \frac{h_1 h_2}{\rho g}^2 \frac{\partial p}{\partial x_1} - \frac{h_1 g_{12}}{\rho g} \frac{\partial p}{\partial x_2} = \frac{1}{\rho} \frac{\partial}{\partial x_3} \left\{ \mu \frac{\partial u_1}{\partial x_3} - \rho \overline{u_1' u_3'} \right\} \qquad (3.2.7)$$

X_2 Momentum Equation

$$\frac{u_1}{h_1} \frac{\partial u_2}{\partial x_1} + \frac{u_2}{h_2} \frac{\partial u_2}{\partial x_2} + u_3 \frac{\partial u_2}{\partial x_3}$$

$$+ u_1 u_1 \frac{h_2}{g} \left\{ \frac{\partial g_{12}}{\partial x_1} - h_1 \frac{\partial h_1}{\partial x_2} - \frac{g_{12}}{h_1} \frac{\partial h_1}{\partial x_1} \right\}$$

$$+ \frac{u_1 u_2}{g} \left\{ h_1 h_2 \left[1 + \left(\frac{g_{12}}{h_1 h_2} \right)^2 \right] \frac{\partial h_2}{\partial x_1} - 2 g_{12} \frac{\partial h_1}{\partial x_1} \right\}$$

$$+ u_2 u_2 \frac{g_{12}}{g} \left\{ \frac{g_{12}}{h_2 h_2} \frac{\partial h_2}{\partial x_2} - \frac{1}{h_2} \frac{\partial g_{12}}{\partial x_2} + \frac{\partial h_2}{\partial x_1} \right\}$$

$$+ 2 \frac{g_{12}}{\sqrt{g}} \omega_3 u_2 + 2 \frac{h_1 h_2}{\sqrt{g}} \omega_3 u_1$$

$$\omega^2 r \frac{h_2 g_{12}}{g} \frac{\partial r}{\partial x_1} - \omega^2 r \frac{h_1^2 h_2}{g} \frac{\partial r}{\partial x_2}$$

$$- \frac{h_2 g_{12}}{\rho g} \frac{\partial p}{\partial x_1} + \frac{h_1^2 h_2}{\rho g} \frac{\partial p}{\partial x_2} = \frac{1}{\rho} \frac{\partial}{\partial x_3} \left\{ \mu \frac{\partial u_2}{\partial x_3} - \rho \overline{u_2' u_3'} \right\} \qquad (3.2.8)$$

Energy Equation

$$\frac{u_1}{h_1} \frac{\partial h_T}{\partial x_1} + \frac{u_2}{h_2} \frac{\partial h_T}{\partial x_2} + u_3 \frac{\partial h_T}{\partial x_3} =$$

$$\frac{1}{\rho} \frac{\partial}{\partial x_3} \left\{ \lambda \frac{\partial t}{\partial x_3} - \rho \overline{u'_3 h_r'} + \mu \frac{\partial}{\partial x_3} \left(\frac{u_T^2}{2} \right) \right\}$$

$$+ \frac{u_1}{2h_1} \frac{\partial}{\partial x_1} (\omega^2 r^2) + \frac{u_2}{2h_2} \frac{\partial}{\partial X_2} (\omega^2 r^2) + \frac{u_2}{2} \frac{\partial}{\partial x_3} (\omega^2 r^2) \qquad (3.2.9)$$

In addition to the equations of motion, we have additional relations which are given below.

Equation of State

$$p = \rho \mathcal{R} t \qquad (3.2.10)$$

Stress/Strain Heat Flux Relations

$$\tau_{13} = \mu \frac{\partial u_1}{\partial x_3} - \rho \overline{u_1' u_3'} = (\mu + \varepsilon_1) \frac{\partial u_1}{\partial x_3} \qquad (3.2.11)$$

$$\tau_{23} = \mu \frac{\partial u_2}{\partial X_3} - \rho \overline{u_2' u_3'} = (\mu + \varepsilon_2) \frac{\partial u_2}{\partial X_3} \qquad (3.2.12)$$

$$\dot{q}_T = \lambda \frac{\partial t}{\partial x_3} - \overline{\rho u_3' h_t'} = \left(\frac{\mu}{Pr} + \frac{\varepsilon_h}{Pr_t}\right) \frac{\partial h_t}{\partial x_3} - \frac{\mu}{Pr} \frac{\partial}{\partial x_3} \left(\frac{u_T^2}{2}\right) \quad (3.2.13)$$

where ε_1 and ε_2 are the nonisotropic components of the eddy viscosity, ε_H is the eddy conductivity, and the turbulent Prandtl number is defined by,

$$P_{rt} = C_p \varepsilon_1 / \varepsilon_H \quad (3.2.14)$$

Total Velocity

$$u_T^2 = u_1^2 + u_2^2 + 2 u_1 u_2 \frac{g_{12}}{h_1 h_2} \quad (3.2.15)$$

where the third term is due to the nonorthogonality of the coordinates.

Total Enthalpy

$$h_T = C_p t + \frac{u_T^2}{2} \quad (3.1.16)$$

Rothalpy

$$i = h_T - v_B^2/2 \quad (3.1.17)$$

where the rotor speed is given by

$$v_B = r\omega \quad (3.2.18)$$

For stationary coordinates, $\omega = 0$ and the rothalpy is identical to the total enthalpy. On a rotating blade, rothalpy is conserved along a streamline. On a stationary blade, total enthalpy is conserved along a streamline. Except for very special cases, it cannot be assumed that the rothalpy is constant over the surface of a rotating blade.

Sutherland's Viscosity Law

$$\mu = \mu_{ref} \left(\frac{t}{t_{ref}}\right)^{3/2} \frac{t_{ref} + 198.6}{t + 198.6} \tag{3.2.19}$$

A number of comments should be made about these equations. First it is noted that these equations are valid only for very thin boundary layers relative to the radius of curvature of the surface. For thick boundary layers on highly curved surfaces a more general coordinate system is required to properly account for the divergence of the streamlines at the edge of the boundary layer. Secondly, it is noted that certain stress terms related to surface curvature are neglected. However, as Bradshaw (Ref. 15) has pointed out, the effects of wall curvature on the generation and decay of turbulence are far larger than the neglected terms. Therefore curvature effects are best treated in the turbulence model. Likewise any effcts of Coriolis forces on the generation and decay of turbulence can also be treated in the turbulence model. Thirdly, it is noted that only one component of the Coriolis force appears in the boundary layer equations. This component is normal to the wall which acts to turn the flow in the x_1 or x_2 direction. For laminar flow, the equations given above form a complete set of equations. For turbulent flow, a turbulence model is required to determine the effective viscosity and conductivity of the flow. The turbulence models used in this study are treated in Section 3.8.

3.3 Normalized Equations

The equations in Section 3.2 are normalized with respect to a reference length (ℓ), a reference velocity (u_∞), and a reference density (ρ_∞). The reference temperature is defined in terms of the reference velocity and the gas constant $\mathcal{R}$. In addition, since the boundary layers are very thin, the coordinate x_3 and the velocity u_3 are scaled by the square root of the Reynolds number. Thus all variables are normalized as follows:

$$\left.\begin{aligned} X_1 &= x_1/\ell \\ X_2 &= x_2/\ell \\ X_3 &= x_3/\ell\sqrt{Re} \end{aligned}\right\} \tag{3.3.1}$$

$$\left.\begin{aligned} U_1 &= u_1/u_\infty \\ U_2 &= u_2/u_\infty \\ U_3 &= u_3/u_\infty\sqrt{Re} \end{aligned}\right\} \tag{3.3.2}$$

$$\left.\begin{aligned} P &= p/(\rho_\infty u_\infty^2) \\ \rho &= \rho/\rho_\infty \\ t_{ref} &= u_\infty^2/\mathcal{R} \\ T &= t/t_{ref} \\ H_T &= h_t/u_\infty^2 \\ I &= i/u_\infty^2 \end{aligned}\right\} \qquad (3.3.3)$$

$$\left.\begin{aligned} \Omega &= \omega\ell/u_\infty \\ R &= r/\ell \end{aligned}\right\} \qquad (3.3.4)$$

$$\left.\begin{aligned} \mu_{ref} &= \mu(t_{ref}) \\ Re &= \rho_\infty u_\infty \ell/\mu_{ref} \\ \mu &= \mu/\mu_{ref} \end{aligned}\right\} \qquad (3.3.5)$$

$$\left.\begin{aligned} H_1 &= h_1/\ell \\ H_2 &= h_2/\ell \\ G_{12} &= g_{12}/\ell^2 \\ |G| &= |g|/\ell^4 \end{aligned}\right\} \qquad (3.3.6)$$

The resulting normalized equations are the same as those given in Seciton 3.2 with lower case letters replaced by upper case letters. The equation of state and the total enthalpy change as follows;

$$P = \rho T \qquad (3.3.7)$$

$$H_T = \frac{\gamma}{\gamma-1} T + \frac{U_T^2}{2} \qquad (3.3.8)$$

3.4 Generalized Levy - Lees Transformation

Boundary layers driven by pressure gradients undergo significant growth or contraction which is difficult to estimate apriori. In addition, turbulent boundary layers have two length scales; an inner length scale near the wall reflecting properties of the law of the wall, and an outer length scale reflecting wake like turbulence behavior. These properties of the turbulent boundary layer make selection of the grid distribution extremely difficult if the flow were solved in physical variables. For laminar two dimensional boundary layers, the Levy-Lees transformation, as given by Blottner (Ref. 9), effectively captures the boundary layer growth thereby significantly simplifying the analysis. For turbulent boundary layers, Werle and Verdon (Ref. 10) have generalized this concept by replacing the laminar edge viscosity coefficient with an effective turbulent viscosity coefficient resulting in a turbulent version of the Levy-Lees transformation. For three dimensional boundary layers, Blottner (Ref. 16) has reviewed some of the transformations currently used. While these transformations work reasonably well for laminar or turbulent flows, they are not entirely satisfactory over the complete range of laminar, turbulent, and transitional flows encountered on gas turbine blades. Vatsa (Ref. 17) has developed a more suitable transformation by extension of the Levy-Lees variables to the three dimensional boundary layer equations. This transformation reduces to those of Blottner (Ref. 9) and Werle and Verdon (Ref. 10) for two dimensional boundary layers. The use of these Levy-Lees variables also has the advantage, which will be exploited in Section 3.7, of allowing the calculation of a family of similarity solutions to be used as inflow conditions for starting the calculation.

The generalized Levy-Lees transformation uses independent variables defined by,

$$\xi_1 = \int_o^{X_1} q_o \, dX_1 \tag{3.4.1}$$

$$\xi_2 = X_2 \tag{3.4.2}$$

$$\xi_3 = \frac{U_{1e} H_2}{\sqrt{2\xi_1}} \int_o^{X_3} \rho \, dX_3 \tag{3.4.3}$$

where

$$q = \rho_e U_{1e} H_1 H_2^2 \mu_e \bar{\varepsilon}_{ref} \tag{3.4.4}$$

$$q_o = q \quad (X_1, 0) \tag{3.4.5}$$

$$\bar{\varepsilon}_1 = 1 + \Gamma\varepsilon/\mu \tag{3.4.6}$$

$$\bar{\varepsilon}_{ref} = 1 + \Gamma\,(\varepsilon/\mu)_e \tag{3.4.7}$$

$$L = \frac{\rho\mu}{\rho_e \mu_e} \tag{3.4.8}$$

The subscript (e) is used to denote the boundary layer edge.

New dependent variables are defined by

$$F = U_1/U_{1e} \tag{3.4.9}$$

$$G = U_2/U_{ref} \tag{3.4.10}$$

$$\Theta = T/T_e \tag{3.4.11}$$

$$H = H_T/H_{Te} \tag{3.4.12}$$

where U_{ref} may be either U_{1e} or U_{2e}. In these new variables a transformed normal velocity is defined by integrating the continuity equation (3.2.6),

$$V = \sqrt{2\xi_1}\,\frac{H_1 H_2}{q}\,\rho_W\,U_{3W}$$

$$-\sqrt{\frac{2\xi_1}{|G|}}\;H_1 H_2\;\frac{q_o}{q}\;\frac{\partial}{\partial\xi_1}\left\{\frac{\sqrt{2\xi_1|G|}}{H_1 H_2}\int_o^{\xi_3} F\,d\,\xi_3\right\}$$

$$-\sqrt{\frac{2\xi_1}{|G|}}\;\frac{H_1 H_2}{q}\;\frac{\partial}{\partial\xi_2}\left\{\frac{\sqrt{2\xi_1|G|}}{H_2^2}\,\frac{U_{ref}}{U_{1e}}\int_o^{\xi_3} G\,d\,\xi_3\right\} \tag{3.4.13}$$

where U_{3W} is the wall injection velocity. The boundary layer equations in the generalized Levy-Lees variables as derived by Vatsa (Ref. 1) are then written as follows:

X_1 Momentum Equation

$$\frac{\partial}{\partial \xi_3}\left[L\,\frac{\bar{\varepsilon}_1}{\bar{\varepsilon}_{ref}}\,\frac{\partial F}{\partial \xi_3}\right] - V\,\frac{\partial F}{\partial \xi_3} - A_1 F\,\frac{\partial F}{\partial \xi_1} - A_2\,G\,\frac{\partial F}{\partial \xi_2}$$

$$- A_{12}\,F^2 - A_{13}\,GF - A_7 G^2 + A_9 F + A_8 G$$

$$+ A_{14}\,\Theta + A_{15} = 0 \qquad (3.4.14)$$

where the coefficients are given by

$$A_1 = 2\xi_1\,q_o/q \qquad (3.4.15)$$

$$A_2 = 2\,\frac{\xi_1}{q}\,\frac{H_1}{H_2}\,\frac{U_{ref}}{U_{1e}} \qquad (3.4.16)$$

$$A_3 = 2\,\xi_1\,\frac{q_o}{q}\,\frac{1}{U_{1e}}\,\frac{\partial U_{1e}}{\partial \xi_1} \qquad (3.4.17)$$

$$A_4 = \frac{2\xi_1}{q}\,\frac{H_1}{H_2}\,\frac{U_{ref}}{U_{1e}}\,\frac{1}{U_{1e}}\,\frac{\partial U_{1e}}{\partial \xi_2} \qquad (3.4.18)$$

$$K_1 = \frac{G_{12}}{H_1^2}\,q_o\,\frac{\partial H_1}{\partial \xi_1} + \frac{\partial H_1}{\partial \xi_2} - \frac{q_o}{H_1}\,\frac{\partial\, G_{12}}{\partial \xi_1} \qquad (3.4.19)$$

$$A_5 = \frac{2\xi_1}{q}\,H_1\,\frac{G_{12}}{|G|}\,K_1 \qquad (3.4.20)$$

$$K_2 = H_1 H_2 \left[1 + \left(\frac{G_{12}}{H_1 H_2} \right)^2 \right] \frac{\partial H_1}{\partial \xi_2} - 2\, G_{12}\, q_o \frac{\partial H_2}{\partial \xi_1} \qquad (3.4.21)$$

$$A_6 = \frac{2\xi_1}{q} \frac{U_{ref}}{U_{1e}} \frac{H_1}{|G|} K_2 \qquad (3.4.22)$$

$$K_3 = \frac{\partial G_{12}}{\partial \xi_2} - H_2 q_o \frac{\partial H_2}{\partial \xi_1} - \frac{G_{12}}{H_2} \frac{\partial H_2}{\partial \xi_2} \qquad (3.4.23)$$

$$A_7 = \frac{2\xi_1}{q} \left(\frac{U_{ref}}{U_{1e}} \right)^2 \frac{H_1{}^2}{|G|} K_3 \qquad (3.4.24)$$

$$A_8 = \frac{4\xi_1}{q} \frac{H_1{}^2}{\sqrt{|G|}} \frac{H_2}{U_{1e}{}^2} U_{ref}\, \Omega_3 \qquad (3.4.25)$$

$$A_9 = \frac{4\xi_1}{q} \frac{H_1 G_{12}}{\sqrt{|G|}} \frac{\Omega_3}{U_{1e}} \qquad (3.4.26)$$

$$A_{10} = \frac{2\xi_1}{q} \frac{H_1{}^2\, H_2{}^2}{|G| U_{1e}{}^2} q_o\, R \frac{\partial R}{\partial \xi_1} \Omega^2 \qquad (3.4.27)$$

$$A_{11} = \frac{2\xi_1}{q} \frac{H_1^2 G_{12}}{|G| U_{1e}^2} R \frac{\partial R}{\partial \xi_2} \Omega^2 \tag{3.4.28}$$

$$A_{12} = A_3 + A_5 \tag{3.4.29}$$

$$A_{13} = A_4 + A_6 \tag{3.4.30}$$

$$A_{14} = A_3 + (A_4 + A_6 - A_8) G_e + A_7 G_e^2 + A_5 - A_9 - A_{10} - A_{11} \tag{3.4.31}$$

$$A_{15} = A_{10} + A_{11} \tag{3.4.32}$$

X_2 Momentum Equation

$$\frac{\partial}{\partial \xi_3} \left[L \frac{\bar{\varepsilon}_2}{\bar{\varepsilon}_{ref}} \frac{\partial G}{\partial \xi_3} \right] - V \frac{\partial G}{\partial \xi_3} - A_1 F \frac{\partial G}{\partial \xi_1} - A_2 G \frac{\partial G}{\partial \xi_2}$$

$$- A_{27} G^2 - A_{28} FG - A_{23} G - A_{20} F^2 - A_{24} F$$

$$+ A_{30} \Theta + A_{29} = 0 \tag{3.4.33}$$

where

$$A_{16} = 2\xi_1 \frac{q_o}{q} \frac{1}{U_{ref}} \frac{\partial U_{2e}}{\partial \xi_1} \tag{3.4.34}$$

$$A_{17} = 2\xi_1 \frac{q_o}{q} \frac{1}{U_{ref}} \frac{\partial U_{ref}}{\partial \xi_1} \tag{3.4.35}$$

$$A_{18} = \frac{2\xi_1}{q} \frac{H_1}{H_2} \frac{U_{2e}}{U_{ref}} \frac{1}{U_{1e}} \frac{\partial U_{2e}}{\partial \xi_2} \tag{3.4.36}$$

$$A_{19} = \frac{2\xi_1}{q} \frac{H_1}{H_2} \frac{1}{U_{1e}} \frac{\partial U_{ref}}{\partial \xi_2} \tag{3.4.37}$$

$$K_4 = q_o \frac{\partial G_{12}}{\partial \xi_1} - H_1 \frac{\partial H_1}{\partial \xi_2} - \frac{G_{12}}{H_1} q_o \frac{\partial H_1}{\partial \xi_1} \tag{3.4.38}$$

$$A_{20} = \frac{2\xi_1}{q} \frac{H_1 H_2}{|G|} \frac{U_{1e}}{U_{ref}} K_4 \tag{3.4.39}$$

$$K_5 = H_1 H_2 \left[1 + \left(\frac{G_{12}}{H_1 H_2}\right)^2\right] q_o \frac{\partial H_2}{\partial \xi_1} - 2 G_{12} \frac{\partial H_1}{\partial \xi_1} \tag{3.4.40}$$

$$A_{21} = \frac{2\xi_1}{q} \frac{H_1}{|G|} K_5 \tag{3.4.41}$$

$$K_6 = \frac{G_{12}}{H_2^2} \frac{\partial H_2}{\partial \xi_2} - \frac{1}{H_2} \frac{\partial G_{12}}{\partial \xi_2} + q_o \frac{\partial H_2}{\partial \xi_1} \tag{3.4.42}$$

$$A_{22} = \frac{2\xi_1}{q} \frac{H_1 G_{12}}{|G|} \frac{U_{ref}}{U_{1e}} K_6 \tag{3.4.43}$$

$$A_{23} = \frac{4\xi_1}{q} \frac{H_1 G_{12}}{\sqrt{|G|}} \frac{\Omega_3}{U_{1e}} \tag{3.4.44}$$

$$A_{24} = \frac{4\xi_1}{q} \frac{H_1^2 H_2}{\sqrt{|G|}} \frac{\Omega_3}{U_{ref}} \tag{3.4.45}$$

$$A_{25} = \frac{2\xi_1}{q} \frac{H_1^2 G_{12}}{|G|} \frac{q_o}{U_{ref}} \frac{\Omega^2}{U_{1e}} R \frac{\partial R}{\partial \xi_1} \tag{3.4.46}$$

$$A_{26} = \frac{2\xi_1}{q} \frac{H_1^2 H_2}{|G|} \frac{\Omega^2}{U_{1e} U_{ref}} R \frac{\partial R}{\partial \xi_2} \tag{3.4.47}$$

$$A_{27} = A_{19} + A_{22} \tag{3.4.48}$$

$$A_{28} = A_{17} + A_{21} \tag{3.4.49}$$

$$A_{29} = A_{26} - A_{25} \tag{3.4.50}$$

$$A_{30} = A_{16} + A_{18} + A_{20} + A_{24} - A_{29} + A_{21} G_e + A_{23} G_e + A_{22} G_e^2 \tag{3.4.51}$$

Energy Equation

$$\frac{\partial}{\partial \xi_3} \left[\frac{L}{Pr} \frac{\bar{\epsilon}_H}{\bar{\epsilon}_{ref}} \frac{\partial H}{\partial \xi_3} \right] - V \frac{\partial H}{\partial \xi_3} - A_1 F \frac{\partial H}{\partial \xi_1} - A_2 G \frac{\partial H}{\partial \xi_2}$$

$$- A_{31} FH - A_{32} GH + A_{33} F + A_{34} G$$

$$+ A_{38} \frac{\partial}{\partial \xi_3} \left[L\ F \frac{\partial F}{\partial \xi_3} \right] + A_{39} \frac{\partial}{\partial \xi_3} \left[LG \frac{\partial G}{\partial \xi_3} \right]$$

$$+ A_{40} \frac{\partial}{\partial \xi_3} \left\{ L\ F \frac{\partial G}{\partial \xi_3} + LG \frac{\partial F}{\partial \xi_3} \right\} = 0 \qquad (3.4.52)$$

where

$$A_{31} = 2\xi_1 \frac{q_o}{q} \frac{1}{H_e} \frac{\partial H_e}{\partial \xi_1} \qquad (3.4.53)$$

$$A_{32} = \frac{2\xi_1}{q} \frac{H_1}{H_2} \frac{U_{ref}}{U_{1e}} \frac{\partial H_e}{\partial \xi_2} \frac{1}{H_e} \qquad (3.4.54)$$

$$A_{33} = 2\xi_1 \frac{q_o}{q} \frac{R}{H_e} \frac{\partial R_e}{\partial \xi_1} \Omega_2^2 \qquad (3.4.55)$$

$$A_{34} = \frac{2\xi_1}{q} \frac{H_1}{H_2} \frac{U_{ref}}{U_{1e}} \frac{R}{H_e} \frac{\partial R}{\partial \xi_2} \Omega^2 \qquad (3.4.56)$$

$$A_{35} = \frac{U_{1e}^2}{H_e} \qquad (3.4.57)$$

$$A_{36} = \frac{U_{ref}^2}{H_e} \qquad (3.4.58)$$

$$A_{37} = \frac{U_{ref}}{U_{1e}} \frac{G_{12}}{H_1 H_2} \qquad (3.4.59)$$

$$A_{38} = A_{35}\left(1 - \frac{1}{Pr}\right)\frac{1}{\bar{\varepsilon}_{ref}} \tag{3.4.60}$$

$$A_{39} = A_{36}\,A_{38} \tag{3.4.61}$$

$$A_{40} = A_{37}\,A_{38} \tag{3.4.62}$$

Continuity Equation

$$\frac{\partial V}{\partial \xi_3} + A_1\frac{\partial F}{\partial \xi_1} + A_2\frac{\partial G}{\partial \xi_2} + A_{45}\,G + A_{46}\,F = 0 \tag{3.4.63}$$

where

$$A_{41} = 2\,\frac{\xi_1}{q}\,\frac{H_1}{H_2}\,\frac{\partial}{\partial \xi_2}\left(\frac{U_{ref}}{U_{1e}}\right) \tag{3.4.64}$$

$$K_7 = \frac{\sqrt{|G|}}{H_2 H_1} \tag{3.4.65}$$

$$A_{42} = \frac{A_1}{K_7}\,\frac{\partial K_7}{\partial \xi_1} \tag{3.4.66}$$

$$K_8 = \frac{\sqrt{|G|}}{H_2^{\,2}} \tag{3.4.67}$$

$$A_{43} = \frac{A_2}{K_8}\,\frac{\partial K_8}{\partial \xi_2} \tag{3.4.68}$$

$$A_{44} = \frac{q_o}{q} \tag{3.4.69}$$

$$A_{45} = A_{41} + A_{43} \tag{3.4.70}$$

$$A_{46} = A_{42} + A_{44} \tag{3.4.71}$$

Additional relations required to complete the set of equations are given by

Equation of State

$$P = \rho T \tag{3.4.72}$$

Turbulent Viscosity Relations

$$\bar{\varepsilon}_1 = 1 + \Gamma\, \varepsilon/\mu \tag{3.4.73}$$

$$\bar{\varepsilon}_2 = 1 + \Gamma\phi\varepsilon/\mu \tag{3.4.74}$$

$$\bar{\varepsilon}_H = 1 + \Gamma \frac{Pr}{Pr_T} \frac{\varepsilon}{\mu} \tag{3.4.75}$$

where Γ is the intermittency factor and ϕ is the ratio of eddy viscosity coefficients if the turbulence is not isotropic. The calculations of these terms depends on the turbulence model which is described in Section 3.8. The total velocity is given by

$$U_T^2 = U_1^2 + U_2^2 + 2 \frac{G_{12}}{H_1 H_2} U_1 U_2 \tag{3.4.76}$$

and the temperature ratio is given by

$$\Theta = \frac{H_T - U_T^2/2}{H_{T_e} - U_{T_e}^2/2} \tag{3.4.77}$$

3.5 Properties of Boundary Layer Equations

The set of equations derived in Section 3.4 consists of four coupled partial differential equations; three of which are second order and one first order. The properties of these equations have been formally examined by Wang (Ref. 18). Wang's analysis shows that these equations are parabolic and therefore may be solved by a forward marching algorithm. However it is noted that there exist two sets of characterstics (see Fig. 4); a set of characteristics which consists of surfaces normal to the wall, and a set of surfaces consisting of the stream surfaces. The set of surfaces normal to the wall are the three dimensional equivalent to the characteristic lines normal to the wall found in the two dimensional boundary layer equations. Thus one may expect that wall and edge boundary conditions must be applied similar to those applied to the two dimensional boundary layer equations. The second set of characteristc surfaces, consisting of stream surfaces, produce the hyperbolic like properties of the three dimensional boundary layer equations. From these surfaces, zones of influence and zones of dependence can be determined as shown by Wang (Ref. 18). These zones are determined by constructing a stream surface from the envelope of streamlines passing through a line perpendicular to the surface at the point in question as shown on Fig. 4. The zone of dependence is given by that volume of space sweeped by all vertical lines passing through the stream surface upstream of the line in question. Likewise the zone of influence is given by that volume of space sweeped by all vertical lines passing through the stream surface downstream of the line in question. Since information is propagated along the characteristic surfaces, the solution for the flow properties on the line in question depends on the flow properties upstream in the zone of dependence. Likewise the flow properties on the line in question influence the flow downstream in the zone of influence. Clearly in a forward marching algorithm, the solution of the flow properties must be known in the zone of dependence in order to calculate the flow on any vertical line. Thus the initial conditions for the problem are all the flow properties on a surface not a stream surface. These initial conditions are called inflow conditions because the solution can be obtained only downstream along stream surfaces. Thus, as pointed out by Blottner (Ref. 16), a unique solution of the three dimensional boundary layer equations requires specification of the inflow conditions along any inflow surface and specification of boundary conditions similar to similar to those employed for the two dimensional boundary layer equations. The boundary conditions are treated in Section 3.6 and the inflow conditions in Section 3.7.

3.6 Boundary Conditions

The boundary conditions are the same as those for the two dimensional compressible boundary layer equations. The no slip condition at the wall takes the form

$$U_1 (X_1, X_2, 0) = 0 \tag{3.6.1}$$

$$U_2 (X_1, X_2, 0) = 0 \tag{3.6.2}$$

With normal injection at the wall we have

$$U_3 (X_1, X_2, 0) = U_W \tag{3.6.3}$$

Where U_W is the surface injection velocity which has been set to zero in the present work. For the energy equation, one may specify either the wall temperature or the heat flux at the wall. Thus we have

$$T (X_1, X_2, 0) = T_W \tag{3.6.4}$$

or

$$\lambda \frac{\partial t}{\partial X_3} = -\dot{q}_w \tag{3.6.5}$$

At the boundary layer edge, we have:

$$\lim_{X_3 \to \infty} U_1 = U_{1e} \tag{3.6.7}$$

$$\lim_{X_3 \to \infty} U_2 = U_{2e} \tag{3.6.8}$$

$$\lim_{X_3 \to \infty} H_T = H_{Te} \tag{3.6.9}$$

In the transformed variables, these boundary conditions take the form

$$F (\xi_1, \xi_2, 0) = 0 \tag{3.6.10}$$

$$G\ (\xi_1,\ \xi_2,\ 0) = 0 \tag{3.6.11}$$

$$V\ (\xi_1,\ \xi_2,\ 0) = \sqrt{2\xi_1}\ \frac{H_1 H_2}{|G|}\ \rho_W\ U_{3W} \tag{3.6.12}$$

$$H\ (\xi_1,\ \xi_2,\ 0) = \frac{\gamma}{\gamma-1}\ \frac{T_W}{H_{Te}} \tag{3.6.13}$$

or

$$\frac{\partial H}{\partial \xi_3}\ (\xi_1,\ \xi_2,\ 0) = -\ \frac{\gamma}{\gamma-1}\ \frac{Pr}{\rho_e U_{1e}\ \sqrt{Re}}\ \frac{\sqrt{2\xi_1}}{H_1}\ \frac{1}{L_W \mu_e H_{Te}}\ \frac{\dot{q}_w}{\rho_\infty u_\infty C_p t_{ref}} \tag{3.6.14}$$

$$F = G = H = 1 \qquad \lim\ \xi_3 \to \infty \tag{3.6.15}$$

Although specification of the boundary conditions Eqs. (3.6.10) through (3.6.15) is sufficient to solve the boundary layer equations, they are not sufficient to solve the problem because the thermodynamic state of the flow is not uniquely specified. This requires that the density and pressure be specified at the edge of the boundary layer. Thus of a complete specification of the problem requires the specification of U_{1e}, U_{2e}, P_e, H_{Te}, ρ_e at the edge of the boundary layer in addition to the above boundary conditions. These quantities are deduced in the present study from a solution of the surface Euler equations subject to the imposed experimental pressure distribution. This analysis is discussed in detail in Section 3.11.

3.7 Inflow Conditions

According to Section 3.5 , the inflow conditions as well as the boundary conditions given in Sect. 3.6 must be specified. These inflow conditions include U_1, U_2, P, T, ρ, H_{Te} along any inflow plane as shown on Fig. 4. These properties may be specified as input data or constructed from analytic relations. In general this data is not known. An alternative approach is to construct the inflow conditions from certain degenerate solutions of the partial differential equations themselves. These degenerate solutions are called similarity solutions and are of two types. The first type, called local similarity solutions, are obtained by reducing the partial differential equations in three independent variables to partial differential equations in two independent variables. Thus, as an example, by setting $\xi_1 = 0$, and solving a set of partial differential equations with ξ_2 and ξ_3 as independent variables, the inflow conditions along

the $\xi_1 = 0$ plane is obtained. The second type of degenerate solutions is obtained by reducing the partial differential equations to ordinary differential equations. These similarity solutions may be called true similarity solutions with one subset the similarity solutions for the two dimensional boundary layer equations. A third special cases does exist for a boundary which is a plane of symmetry for the flow field. In this last case, the plane of symmetry is a characteristic surface and requires special treatment as will be shown below.

Local Similarity Solutions

For local similarity solutions, the inflow conditions are only a function of ξ_1 and ξ_3 along a ξ_2 boundary and only a function of ξ_2 and ξ_3 along a ξ_1 boundary. An inspection of the differential equations in Section 3.4 indicates that these solutions can be obtained by setting

$$A_1 = 0 \text{ along a } \xi_1 = \text{const. boundary}$$

$$A_2 = 0 \text{ along a } \xi_2 = \text{const. boundary} \qquad (3.7.1)$$

and using the local edge conditions.

True Similarity Solutions

One subset of true similarity solutions is for two dimensional incompressible laminar flow. For this subset it is assumed that:

$$dS_1 = H_1 dX_1 \qquad (3.7.2)$$

$$S_2 = H_2 X_2 \qquad (3.7.3)$$

$$G_{12} = 0 \qquad (3.7.4)$$

$$U_{1e} = U_{1eo} S_1^{\,m} \qquad (3.7.5)$$

$$U_{2e} = 0 \qquad (3.7.6)$$

$$H_{Te} = H_{Te0} \qquad (3.7.7)$$

Note that these solutions require orthogonality of coordinates at the inflow plane and require a power law expansion of the velocity edge conditions. With these assumptions the differential equations of Section 3.4 , reduce to a set of ordinary differential equations where all coefficients $A_n = 0$ except

$$A_3 = \frac{2m}{m+1} = \beta$$

$$A_{17} = \frac{2m}{m+1} = \beta \qquad (3.7.8)$$

$$A_{28} = \frac{2m}{m+1} = \beta$$

$$A_{36} = 1$$

$$A_{44} = 1$$

$$A_{46} = 1$$

The equations of Section 3.4 reduce to the well known Falkner-Skan equations of which two solutions are of special interest.

$$\beta = 0 \quad \text{Flat Plate Solution}$$
$$\qquad (3.7.9)$$
$$\beta = 1 \quad \text{Stagnation Point Solution}$$

Although these true similarity solutions were not used in the present study, they have general usefulness in a variety of real problems. As an example on a cascade of blades with no spanwise pressure gradient, the Falkner-Skan solution with $\beta = 1$ can start the calculation at the leading edge stagnation point.

Plane of Symmetry Solution

Since no flow crosses a plane of symmetry, a plane of symetry is a characteristic surface and the solution of the equations are indeterminate. Blottner (Ref. 19) has derived the special relations needed to resolve the

indeterminancy in the equations. Across a plane of symmetry ($X_2 = 0$) the following conditions apply:

$$\vec{\Omega} = 0 \tag{3.7.10}$$

$$\begin{aligned} P\ (X_1, X_2) &= P\ (X_1, -X_2) \\ T\ (X_1, X_2) &= T\ (X_1, -X_2) \\ U_1\ (X_1, X_2) &= U_1(X_1, -X_2) \\ U_2\ (X_1, X_2) &= -U_2\ (X_1, -X_2) \end{aligned} \tag{3.7.11}$$

Clearly from Eq. (3.7.11)

$$U_2\ (X_1, 0) = 0 \tag{3.7.12}$$

In addition to the flow variables having symmetry, the coordinates, the metrics, and the surface should have symmetry.

$$G_{12} = 0 \tag{3.7.13}$$

$$\frac{\partial H_1}{\partial X_2} = \frac{\partial H_2}{\partial X_2} = 0 \tag{3.7.14}$$

Then following the method of Blottner (Ref. 19), the solution is expanded in a power series in X_2 and keeping only the first term results in,

$$U_{ref} = U_{2e} = \left(\frac{\partial U_{2e}}{\partial X_2}\right)_o X_2 \tag{3.7.15}$$

where the subscript (o) refers to the first term of the Taylor series expansion,

such that

$$\lim_{\xi_3 \to \infty} \mathfrak{F}(\xi_3) = 1 \tag{3.7.16}$$

Then by inspection of the equations in Section 3.4, the nonzero coefficients in the boundary layer equations are given by

$$A_1 = 2\xi_1$$

$$A_3 = \frac{2\xi_1}{q_o} \frac{1}{U_{1e}} \frac{\partial U_{1e}}{\partial \xi_1}$$

$$A_{12} = A_3$$

$$A_{14} = A_3$$

$$A_{16} = 2 \frac{\xi_1}{q_o} \frac{\partial}{\partial X_1} \left\{ \ell n \left[\frac{\partial U_{2e}}{\partial X_2} \right] \right\}_0 \tag{3.7.17}$$

$$A_{17} = A_{16}$$

$$A_{18} = \frac{\xi_1}{q_o} \frac{H_1}{H_2} \frac{1}{U_{1e}} \left[\frac{\partial U_{2e}}{\partial X_2} \right]_0$$

$$A_{19} = A_{18}$$

$$A_{27} = A_{19}$$

$$A_{28} = A_{17}$$

$$A_{30} = A_{16} + A_{18}$$

$$A_{31} = \frac{2\xi_1}{q_o} \frac{1}{H_{Te}} \frac{\partial H_{Te}}{\partial X_1}$$

$$A_{41} = A_{18}$$

$$A_{44} = 1 \qquad (3.7.18)$$

$$A_{44} = 1$$

$$A_{45} = A_{41}$$

$$A_{46} = A_{42} + A_{44}$$

Note that the expansion of U_{2e} removes the indeterminancy in the coefficients A_{16} and A_{18}.

3.8 Turbulence Model

The turbulence model used by Vatsa (Ref. 1) is based on the Cebeci and Smith model (Ref. 20) developed for two dimensional boundary layers. This model may be extended to three dimensional boundary layer flow by replacing the streamwise velocity with the total velocity. Thus in the inner region we have

$$\left(\frac{\varepsilon}{\mu}\right)_i = \frac{\rho}{\mu} \left(\ell_m\right)^2 \frac{\partial u_T}{\partial x_3} \qquad (3.8.1)$$

where the derivative of the total velocity and the mixing length are given by

$$\frac{\partial u_T}{\partial x_3} = \left\{ \left(\frac{\partial u_1}{\partial x_3}\right)^2 + \left(\frac{\partial u_2}{\partial x_3}\right)^2 + \frac{2G_{12}}{h_1 h_2} \frac{\partial u_1}{\partial x_3} \frac{\partial u_2}{\partial x_2} \right\}^{1/2} \qquad (3.8.2)$$

$$\ell_m = \kappa x_3 \left[1 - \exp\left(\frac{-x_3}{A}\right)\right] \tag{3.8.3}$$

where κ is the Von Karman constant generally taken to be 0.4. The coefficient in the damping factor is given by

$$A = 26 \frac{\mu_w}{\rho_w u^*} \left(\frac{\rho}{\rho_w}\right)^{1/2} \tag{3.8.4}$$

where

$$u^* = (\tau_w/\rho_w)^{1/2} \tag{3.8.5}$$

$$\tau_w = \mu_w \left(\frac{\partial u_T}{\partial x_3}\right)_w \tag{3.8.6}$$

In the outer region, the eddy viscosity is given by the Clauser model in the form

$$\frac{\varepsilon}{\mu}_0 = \chi \frac{\rho}{\mu} \ell_o \tag{3.8.7}$$

where ℓ_o is a representative length scale and χ is the Clauser constant generally taken to be 0.016. The outer layer length scale, as developed by Mellor and Herring (Ref. 21), is taken to be

$$\ell_o = \int_0^\infty x_3 \frac{\partial u}{\partial x_3} dx_3 \tag{3.8.8}$$

The intermittency factor Γ is used to model laminar/turbulent transitional flow and varies between the limits 0.0 and 1.0. Since a transition model does not exist for three dimensional boundary layers, the simplest forced transition model for two dimensional flow is used. This model is that developed by Dhawan and Narasimha (Ref. 22) which is given by

$$\Gamma = 1 - \exp\left[-4.6513\left(\frac{S - S_{T1}}{S_{T2} - S_{T1}}\right)^2\right] \qquad (3.8.9)$$

where S_{T1} and S_{T2} are the specified locations for the beginning and end of transition. Finally we note that three dimensional turbulent boundary layers may have nonisotropic turbulence. Thus the eddy viscosity in the cross flow direction is multiplied by a factor ϕ which may take a value as low as 0.40.

3.9 Finite Difference Equations

The governing equations described in Section 3.4 are a set of four coupled nonlinear partial differential equations. These equations are reduced by Vatsa (Ref. 2) to a set of four coupled nonlinear finite difference equations using the finite difference operators given below.

$$\frac{\partial Q}{\partial \xi_1} = (Q^K_{I,J} - Q^K_{I-1,J})/(\xi_{1,I} - \xi_{1,I-1}) \qquad (3.9.1)$$

$$\frac{\partial Q}{\partial \xi_2} = (Q^K_{I,J} - Q^K_{I,J-1})/(\xi_{2,J} - \xi_{2,J-1}) \qquad U_2 > 0 \qquad (3.9.2)$$

$$= (Q^K_{I-1,J+1} - Q^K_{I-1,J})/(\xi_{2,J+1} - \xi_{2,J}) \quad U_2 < 0 \qquad (3.9.3)$$

$$\frac{\partial Q}{\partial \xi_3} = (Q^{K+1}_{I,J} - Q^{K-1}_{I,J})/(\xi_3^{K+1} - \xi_3^{K-1}) \qquad (3.9.4)$$

$$\frac{\partial}{\partial \xi_3}\left[\varepsilon \frac{\partial Q}{\partial \xi_3}\right] = \frac{\varepsilon^K + \varepsilon^{K+1}}{\xi_3^{K+1} - \xi_3^{K-1}} \cdot \frac{Q^{K+1}_{I,J} - Q^K_{I,J}}{\xi_3^{K+1} - \xi_3^K}$$

$$- \frac{\varepsilon^K + \varepsilon^{K-1}}{\xi_3^{K+1} - \xi_3^{K-1}} \cdot \frac{Q^K_{I,J} - Q^{K-1}_{I,J}}{\xi_3^K - \xi_3^{K-1}} \qquad (3.9.5)$$

where Q represents a general solution vector (F, G, V, H) and the i, j, k subscripts refer to the streamwise ξ_1, spanwise ξ_2, and normal ξ_3 locations respectively. Note that upwind difference is used on the crossflow convective derivatives depending on the sign of the crossflow velocity so as to honor the region of dependence criteria. When the crossflow velocity is negative, the differencing is explicit and there is a stability criteria on the step size which must be satisified.

$$\frac{U_1}{U_2} < -\frac{H_1 \Delta X_1}{H_2 \Delta X_2} \tag{3.9.6}$$

The resulting nonlinear difference equations are quasi-linearized to form a set of linear matrix equations which are solved in an iterative fashion (see Vatsa, Refs. 1 and 2). The matrix equations are solved by a block substitution algorithm described in detail by Vatsa (Ref. 2).

3.10 Generalized Surface Coordinates

The computational coordinates are surface coordinates that wrap around the blade surface such that when $X^3 = 0.0$, any point on the surface is a function of only X^1 and X^2. Furthermore the computational domain shall be arbitrarily bounded by

$$0.0 \leq X^1 \leq 1.0$$
$$0.0 \leq X^2 \leq 1.0 \tag{3.10.1}$$

without any loss of generality and as assumed in Section 3.1, the coordinate X^3 shall be normal to the surface and hence normal to both X^1 and X^2. The coordinates of the physical surface (Y_1, Y_2, Y_3) are generally known only in Cartesian coordinates. Therefore we shall use the Cartesian coordinates as the basis for the transformation. (Note subscripts and superscripts are used to denote covariant and contravariant tensor components respectively.) The purpose of this section is to find a general tensor transformation from the computational coordinates $(\vec{X})$ to the physical (Cartesian) coordinates $(\vec{Y})$ for an arbitrary surface. It shall be noted at the outset that the Cartesian coordinates of the surface are generally not known in analytical form but only in numerical form so that a

general surface spline fitting algorithm is required to construct the transformation. Thus we are searching for a transformation of the form

$$\vec{Y} = \vec{Y}\,(\vec{X}) \tag{3.10.2}$$

having the above properties and such that the Jacobian

$$J = \left|\frac{\partial Y_i}{\partial X^j}\right| \neq 0 \tag{3.10.3}$$

within the computational domain. A nonorthogonal coordinate system having these properties can always be constructed provided that the surface projects uniquely to a plane surface. Thus if one projects all points on the surface onto the $Y_3 = 0.0$ plane such that Eq. (3.10.3) is satisfied, then uniqueness is assured. Under these conditions, (see Fig. 2), the Cartesian coordinates of the surface $(\vec{Y})$ can be written in parametric form using only the computational coordinates $X^1, X^2)$. The transformation, Eq. (3.10.2), then takes the special form

$$Y_1 = Y_1\,(X^1, X^2) \tag{3.10.4}$$

$$Y_2 = Y_2\,(X^1, X^2) \tag{3.10.5}$$

$$Y_3 = Y_3\,[Y_1(X^1, X^2),\ Y_2\,(X^1, X^2)\,] \tag{3.10.6}$$

It is noted that if the transformations Eq. (3.10.4) and (3.10.5) are known, then the equation of the surface in the physical coordinates is known in terms of the computational coordinates by direct substitution via Eq. (3.10.6). The task then is to determine the transformations given by Eqs. (3.10.4) and (3.10.5). From Fig. 2, it is noted that the four boundaries projected onto the $Y_3 = 0.0$ plane correspond to

$$\begin{aligned} X^1 &= 0.0 \quad \text{side 1} \\ X^2 &= 0.0 \quad \text{side 4} \\ X^1 &= 1.0 \quad \text{side 3} \\ X^2 &= 1.0 \quad \text{side 2} \end{aligned} \tag{3.10.7}$$

Thus, as an example, the Cartesian coordinates of the side 1 boundary can be written in terms of only X^2 as a parameter. Since these boundaries are known only at descrete points in the form of numerical data, the side 1 boundary can parametized with X^2 as a variable using the following procedure for N boundary points.

$$Y_1\ (0,\ X^2) = Y_1\ [X^2\ (I)]_{\text{side 1}} = Y_1(I)_{\text{side 1}}$$

$$Y_2\ (0,\ X^2) = Y_2\ [X^2(I)]_{\text{side 1}} = Y_2(I)_{\text{side 2}} \qquad (3.10.8)$$

$$X^2\ (I) = (I-1)/(N-1)\quad I = 1,\ N$$

Thus to each pair of points $Y_1(I)$, $Y_2\ (I)$ there corresponds a unique $X^2(I)$. A similar proceedure is followed on the remaining three sides. With the four boundaries written in parametric form with the appropriate X^1 or X^2 as a variable, any interior point is uniquely calculated using the transfinite mapping of Gordon and Thiel (Ref. 5).

$$\begin{aligned} Y_i\ (X^1;\ X^2) &= (1-X^1)\ Y_i(0,\ X^2) + X^1\ Y_i\ (1,\ X^2) \\ &+ (1 - X^2)\ Y_i\ (X^1;\ 0) + X^2 Y_i\ (X^1;\ 1) \\ &- (1-X^1)(1-X^2)\ Y_i\ (0,\ 0) - (1-X^1)X^2 Y_i(0,1) \qquad (3.10.9) \\ &- X^1(1-X^2)\ Y_i\ (1,0) - X^1X^2\ Y_i(1,1) \end{aligned}$$

where i = 1,2. Then given any X^1 and X^2, the Cartesian coordinates (Y_1, Y_2, Y_3) are determined uniquely using Eqs. (3.10.9) and Eq. (3.10.6). The covariant metric tensor components are then determined from

$$G_{ij} = \frac{\partial Y_k}{\partial X_i}\ \frac{\partial Y_k}{\partial X_j} \qquad (3.10.10)$$

$$H_1 = \sqrt{G_{11}} \tag{3.10.11}$$

$$H_2 = \sqrt{G_{22}}$$

$$H_3 = 1$$

$$|G| = \det|G_{ij}| \tag{3.10.12}$$

where the contravarient tensor notation is dropped for Eqs. (3.10.10) through (3.10.12). We note the the covariant metric tensor components (see Eq. (3.10.10)) require first derivatives and also that the equations of motion requires derivatives of of the metric tensor (see Section 3.2). Therefore first and second derivatives of the the transformation Eq. (3.10.2) are required. Interpolation and differentiation of the boundary curves is done using a four point Lagrangian interpolation formula. Interpolation and differentiation of Eq. (3.10.6) is done using a surface spline fit developed by McCartin (Ref. 23) and Spath (Ref. 24).

In addition to the metric tensor components G_{ij}, the boundary layer equations also require components of the coordinate rotation vector Ω (see Section 3.2). In addition it is usefull to be able to resolve any vector in the computational coordinates to the corresponding vector in the Cartesian coordinates. Therefore the direction cosines from the computational to Cartesian coordinates must be determined. In the present work these direction cosines are used to resolve Cartesian components of the boundary layer edge velocities and the wall shear force vector. A vector in Cartesian space is given by

$$\vec{dR} = \vec{e}_1 dY^1 + \vec{e}_2 dY^2 + \vec{e}_3 dY^3 \tag{3.10.13}$$

where $\vec{e}_i$ is the unit Cartesian vector. However on the surface, from Eq. (3.10.6)

$$dY^3 = \frac{\partial Y^3}{\partial Y^1} dY^1 + \frac{\partial Y^3}{\partial Y^2} dY^2 \tag{3.10.14}$$

hence Eq. (3.10.13) becomes

$$\vec{dR} = \vec{e}_1 dY^1 + \vec{e}_2 dY^2 + \vec{e}_3 \left[\frac{\partial Y^3}{\partial Y^1} \, dY^1 + \frac{\partial Y^3}{\partial Y^2} \, dY^2 \right] \tag{3.10.15}$$

On the surface $X^3 = 0.0$ and

$$dY^1 = \frac{\partial Y^1}{\partial X^1} \, dX^1 + \frac{\partial Y^1}{\partial X^2} \, dX^2$$

$$dY^2 = \frac{\partial Y^2}{\partial X^1} \, dX^1 + \frac{\partial Y^2}{\partial X^2} \, dX^2 \tag{3.10.16}$$

Substituting Eq. (3.10.16) into Eq. (3.10.15), we have

$$\vec{dR} = \left[\vec{e}_1 \frac{\partial Y^1}{\partial X^1} + \vec{e}_2 \frac{\partial Y^2}{\partial X^1} + \vec{e}_3 \left(\frac{\partial Y^3}{\partial Y^1} \frac{\partial Y^1}{\partial X^1} + \frac{\partial Y^3}{\partial Y^2} \frac{\partial Y^2}{\partial X^1} \right) \right] dX^1$$

$$+ \left[\vec{e}_1 \frac{\partial Y^1}{\partial X^2} + \vec{e}_2 \frac{\partial Y^2}{\partial X^2} + \vec{e}_3 \left(\frac{\partial Y^3}{\partial Y^1} \frac{\partial Y^1}{\partial X^2} + \frac{\partial Y^3}{\partial Y^2} \frac{\partial Y^2}{\partial X^2} \right) \right] dX^2 \tag{3.10.17}$$

The contravariant components of $\vec{dR}$ can also be written as

$$\vec{dR} = \vec{a}_1 dX^1 + \vec{a}_2 dX^2 + \vec{a}_3 (0) \tag{3.10.18}$$

with $\vec{a}$ as the basis vector and noting that $dX^3 = 0$ on the surface. Hence by comparing terms between Eqs. (3.10.17) and (3.10.18) we have

$$\vec{a}_1 = \vec{e}_1 \frac{\partial Y^1}{\partial X^1} + \vec{e}_2 \frac{\partial Y^2}{\partial X^1} + \vec{e}_3 \left[\frac{\partial Y^3}{\partial Y^1} \frac{\partial Y^1}{\partial X^1} + \frac{\partial Y^3}{\partial Y^2} \frac{\partial Y^2}{\partial X^1} \right]$$

(3.10.19)

$$\vec{a}_2 = \vec{e}_1 \frac{\partial Y^1}{\partial X^2} + \vec{e}_2 \frac{\partial Y^2}{\partial X^2} + \vec{e}_3 \left[\frac{\partial Y^3}{\partial Y^1} \frac{\partial Y^1}{\partial X^2} + \frac{\partial Y^3}{\partial Y^2} \frac{\partial Y^2}{\partial X^2} \right]$$

The unit vectors then become

$$\vec{n}_1 = \frac{\vec{e}_1}{H_1} \frac{\partial Y_1}{\partial X_1} + \frac{\vec{e}_2}{H_1} \frac{\partial Y_2}{\partial X_1} + \frac{\vec{e}_3}{H_1} \left[\frac{\partial Y_3}{\partial Y_1} \frac{\partial Y_1}{\partial X_1} + \frac{\partial Y_3}{\partial Y_2} \frac{\partial Y_2}{\partial X_1} \right]$$

(3.10.20)

$$\vec{n}_2 = \frac{\vec{e}_1}{H_2} \frac{\partial Y_1}{\partial X_2} + \frac{\vec{e}_2}{H_2} \frac{\partial Y_2}{\partial X_2} + \frac{\vec{e}_3}{H_2} \left[\frac{\partial Y_3}{\partial Y_1} \frac{\partial Y_1}{\partial X_2} + \frac{\partial Y_3}{\partial Y_2} \frac{\partial Y_2}{\partial X_2} \right]$$

$$\vec{n}_3 = \vec{n}_1 \times \vec{n}_2 / |\vec{n}_1 \times \vec{n}_3|$$

where the distinction between covariant and contravariant vectors may be dropped. The direction cosines are then given by

$$\gamma_{ij} = \vec{n}_i \cdot \vec{e}_j \qquad (3.10.21)$$

Then if U_i is any vector in the X_i direction in the computational coordinates and V_j is any vector in the Cartesian coordinates, then

$$V_j = \gamma_{ij}\, U_i$$

$$U_j = \gamma_{ij}^{-1}\, V_i \qquad (3.10.22)$$

3.11 Surface Euler Equations

The solution of the boundary layer equations requires specification of the edge conditions (U_{1e}, U_{2e}, H_{Te}, ρ_e, P_e) as shown in Section 3.5. These edge conditions can be obtained directly from experimental data or they can be obtained from solutions of the Euler equations. An alternative method is to solve the surface Euler equations using a known surface static pressure distribution. This method was outlined by Cebeci et al. (Ref. 7) for application to aircraft wings. Gleyzes and Coustiex (Ref. 8) developed a similar method for incompressible flow over fusiform bodies. This section extends these methods to obtain a solution of the compressible surface Euler equations for application to arbitrary three dimensional surface such as turbine blades.

The surface Euler equations can be obtained from the three dimensional boundary layer equations given in Section 3.2 by taking the limit as $X_3 \to \infty$. Thus at the edge of the boundary layer normal derivatives vanish and hence the momentum and energy equations are written as follows:

X_1 Momentum

$$\frac{U_{1e}}{H_1}\frac{\partial U_{1e}}{\partial X_1} + \frac{U_{2e}}{H_2}\frac{\partial U_{1e}}{\partial X_2} + a_1 U_{1e}^2 + a_2\, U_{1e}\, U_{2e} + a_3 U_{2e}^2 + C_1 U_{1e} + C_2 U_{2e} + C_3 = a_4 \frac{\partial C_P}{\partial X_1} + a_5 \frac{\partial C_P}{\partial X_2} \qquad (3.11.1)$$

X_2 Momentum

$$\frac{U_{1e}}{H_1}\frac{\partial U_{2e}}{\partial X_1} + \frac{U_{2e}}{H_2}\frac{\partial U_{2e}}{\partial X_2} + a_6 U_{1e}^2 + a_7\, U_{1e}\, U_{2e} + a_8 U_{2e}^2 + C_4 U_{1e} + C_5 U_{2e} + C_6 = a_9 \frac{\partial C_P}{\partial X_1} + a_{10} \frac{\partial C_P}{\partial X_2} \qquad (3.11.2)$$

Energy

$$\frac{U_{1e}}{H_1}\frac{\partial I_e}{\partial X_1} + \frac{U_{1e}}{H_2}\frac{\partial I_e}{\partial X_2} = 0 \qquad (3.11.3)$$

The coefficients in these equations are given by

$$a_1 = \frac{G_{12}}{|G|}\left\{\frac{G_{12}}{H_1^2}\frac{\partial H_1}{\partial X_1} + \frac{\partial H_1}{\partial X_2} - \frac{1}{H_1}\frac{\partial G_{12}}{\partial X_1}\right\}$$

$$a_2 = \frac{1}{|G|}\left\{H_1H_2\left[1 + \left(\frac{G_{12}}{H_1H_2}\right)^2\right]\frac{\partial H_1}{\partial X_2} - 2G_{12}\frac{\partial H_2}{\partial X_1}\right\}$$

$$a_3 = \frac{H_1}{|G|}\left\{\frac{\partial G_{12}}{\partial X_2} - H_2\frac{\partial H_2}{\partial X_1} - \frac{G_{12}}{H_2}\frac{\partial H_2}{\partial X_2}\right\}$$

$$a_4 = -\frac{H_1H_2^2}{2|G|}\frac{1}{\rho}$$

$$a_5 = -\frac{H_1^2G_{12}}{2|G|}\frac{1}{\rho}$$

$$a_6 = \frac{H_{12}}{|G|}\left\{\frac{\partial G_{12}}{\partial X_1} - H_1\frac{\partial H_1}{\partial X_2} - \frac{G_{12}}{H_1}\frac{\partial H_1}{\partial X_1}\right\}$$

$$a_7 = \frac{1}{|G|}\left\{H_1H_2\left[1+\left(\frac{G_{12}}{H_1H_2}\right)^2\right]\frac{\partial H_2}{\partial X_1} - 2G_{12}\frac{\partial H_1}{\partial X_2}\right\}$$

$$a_8 = \frac{G_{12}}{|G|}\left\{\frac{G_{12}}{H_2{}^2}\frac{\partial H_2}{\partial X_2} + \frac{\partial H_2}{\partial X_1} - \frac{1}{H_2}\frac{\partial G_{12}}{\partial X_2}\right\}$$

$$a_9 = -\frac{H_2G_{12}}{2|G|}\frac{1}{\rho}$$

$$a_{10} = -\frac{H_1{}^2H_2}{2|G|}\frac{1}{\rho}$$

$$C_1 = -\frac{2G_{12}}{\sqrt{|G|}}\Omega_3$$

$$C_2 = -\frac{2H_1H_2}{\sqrt{|G|}}\Omega_3$$

$$C_3 = -R\Omega^2\frac{H_1H_2{}^2}{|G|}\left\{\frac{\partial R}{\partial X_1} - \frac{H_1G_{12}}{|G|}\frac{\partial R}{\partial X_2}\right\}$$

$$C_4 = \frac{2H_1H_2}{\sqrt{|G|}}\Omega_3$$

$$C_5 = \frac{2G_{12}}{\sqrt{|G|}} \Omega_3$$

$$C_6 = R\Omega^2 \left\{ \frac{H_2 G_{12}}{|G|} \frac{\partial R}{\partial X_1} - \frac{H_1{}^2 H_2}{|G|} \frac{\partial R}{\partial X_2} \right\}$$

The static pressure has been expressed in terms of the pressure coefficient defined as

$$C_P = \frac{P - P_\infty}{\frac{1}{2} \rho_\infty u_\infty{}^2} = 2 (P - P_\infty) \qquad (3.11.4)$$

since experimental data is normally given in this form.

Inflow Conditions

The solution of these equations requires specification of the velocity components U_{1e} and U_{2e} as well as the thermodynamic variables P_e, T_e, ρ_e along the inflow boundaries. In general, only the local surface static pressure coefficient and the freestream or reference stagnation conditions $P_{T\infty}$ and $T_{T\infty}$ are known. If the local flow angle can be estimated, then the local edge conditions can be calculated by expanding the flow isentropically from the known stagnation conditions to the local measured static pressure.

A useful relation for this purpose is one between the pressure coefficient and velocity. For incompressible flow this is given by the Bernoulli equation. Since on a rotor the total pressure and total temperature are not constant for the whole flow field, they are assumed constant along a surface of constant radius. (The Bernoulli surfaces are cylindrical surfaces). Thus P_T and T_T are a function of radius and we have

$$\tilde{P}_T = P + \frac{\rho}{2} \underset{\sim}{\vec{U}}_e \cdot \underset{\sim}{\vec{U}}_e \qquad (3.11.5)$$

where

$$\underset{\sim}{\vec{U}}_e \cdot \underset{\sim}{\vec{U}}_e = \vec{U}_e \cdot \vec{U}_e + 2\,\vec{U}_e \cdot (\vec{\Omega} \times \vec{R}) + (\Omega R)^2 \qquad (3.11.6)$$

If the vorticity is aligned with the Y_1 axis and the radius vector is aligned with the Y_2 axis, then

$$\vec{U}_e \cdot (\vec{\Omega} \times \vec{R}) = (\Omega R)\left(\gamma_{13}U_{1e} + \gamma_{23}U_{2e}\right) \qquad (3.11.7)$$

Likewise the reference conditions are given by

$$P_{T\infty} = P_\infty + \frac{\rho_\infty}{2}\,\underset{\sim}{\vec{U}}_\infty \cdot \underset{\sim}{\vec{U}}_\infty \qquad (3.11.8)$$

$$\underset{\sim}{\vec{U}}_\infty \cdot \underset{\sim}{\vec{U}}_\infty = \vec{U}_\infty^2 + 2\,(R\Omega)_\infty U_{\phi\infty} + (\Omega R)^2 \qquad (3.11.9)$$

Combining these equations results in an explicit relation between C_p and $\vec{U}_e$.

$$U_{1e}^2 + a_o\,U_{1e}U_{2e} + U_{2e}^2 + d_1U_{1e} + d_2U_{2e} = 1 - C_p + d_o + d_4 + d_5 \qquad (3.11.10)$$

where it is noted that $\rho = \rho_\infty = 1$ and $U_\infty = 1$ for incompressible flow. For compressible flow, the same reasoning applies. Thus total pressure and total temperature are constant along cylindrical surfaces and

$$\frac{P_T}{P} = \left\{1 + \frac{\gamma-1}{2}\,\frac{\underset{\sim}{\vec{U}} \cdot \underset{\sim}{\vec{U}}}{a^2}\right\}^{\frac{\gamma}{\gamma-1}} \qquad (3.11.11)$$

The energy equation can be written as

$$a_T^2 = a^2 + \frac{\gamma-1}{2} \tilde{\vec{U}} \cdot \tilde{\vec{U}} \qquad (3.11.12)$$

and combining the equations we have,

$$U_{1e}^2 + U_{2e}^2 + 2a_o U_{2e} + d_1 U_{1e} + d_2 U_{2e} = d_8 + d_9 \qquad (3.11.13)$$

where the coefficients are given by

$$d_1 = 2\Omega R \gamma_{13}$$

$$d_2 = 2\Omega R \gamma_{23}$$

$$d_3 = 1 - C_P$$

$$d_4 = (\Omega R)_\infty^2 - (\Omega R)^2$$

$$d_5 = (\Omega R)_\infty^2 - (\Omega R)^2$$

$$d_7 = \left\{ \frac{2}{\gamma-1} \left(\frac{P_T}{P} \right)^{\frac{\gamma-1}{\gamma}} - 1 \right\}$$

$$d_8 = \frac{d_7 a_T^2}{1 + \frac{\gamma-1}{2} d_7}$$

$$d_9 = (\Omega R)^2$$

$$d_o = 2\ (\tilde{P}_T - \tilde{P}_{T\infty})$$

$$a_o = 2G_{12}/(H_1 H_2)$$

Auxiliary Relations

Three additional relations are required to complete the set of equations. These are the equation of state

$$P = \rho_e\ T_e \tag{3.11.14}$$

and the equations for total enthalpy and rothalpy

$$H_{Te} = \frac{\gamma}{\gamma-1}\ T_e + \frac{U_{Te}^2}{2} \tag{3.11.15}$$

$$I_e = H_{Te} - \frac{V_B^{\ 2}}{2} \tag{3.11.16}$$

Solution Algorithm

These equations are hyperbolic equations in which the characteristics are the streamlines. Therefore these equations have the same properties as the boundary layer equations discussed in Section 3.5 and are solved by specifying the inflow conditions on the inflow boundary. These inflow conditions are given by (U_{1e}, U_{2e}, H_{Te}, P_e). Since pressure (i.e., C_P) is a known input, the velocity components U_{1e} and U_{2e} may be determined by specifying either U_{2e} or the flow angle on the inflow plane and using Eq. (3.11.10) or (3.11.13) to determine U_{1e}. With the velocities known, the temperature is determined from Eq.(3.11.14) and Eq.(3.11.15). Finally the density is determined from Eq.(3.11.14).

These equations have the same properties as the boundary layer equations and the finite difference equations are formed in the same manner using the Eqs. (3.9.1), (3.9.2) and (3.9.3). This results in a set of coupled algebraic equations.

$$b_1 U_{1e}^2 + b_2 U_{1e} + b_3 U_{1e} U_{2e} + b_4 U_{2e} + b_5 U_{2e}^2 + b_6 = 0 \qquad (3.11.17)$$

$$b_7 U_{1e}^2 + b_8 U_{1e} + b_9 U_{1e} U_{2e} = b_{10} U_{2e} + b_{11} U_{2e}^2 + b_{12} = 0 \qquad (3.11.18)$$

$$e_4 I_e = e_5 \qquad (3.11.19)$$

where the coefficients are given by

$U > 0.0$	$U < 0.0$
$a_{11} = 1/(H_1 \Delta X_{1,I-1})$	$a_{11} = 1/H_1 \Delta X_{1,I-1})$
$a_{12} = 1/(H_2 \Delta X_{2,J-1})$	$a_{12} = 1/(H_2 \Delta X_{2,J})$

$$a_{13} = a_4 \frac{\partial C_P}{\partial X_1} + a_5 \frac{\partial C_P}{\partial X_2}$$

$$a_{14} = a_9 \frac{\partial C_P}{\partial X_1} + a_{10} \frac{\partial C_P}{\partial X_2}$$

$b_1 = a_{11} + a_1$	$b_1 = a_{11} + a_1$
$b_2 = a_{11} U_{1e,I-1} + C_1$	$b_2 = - a_{11} U_{1e,I-1,J} + C_1$
$b_3 = a_{12} + a_2$	$b_3 = a_2$
$b_4 = a_{12} U_{1e,I,J-k} + C_2$	$(b_4 = a_{12} (U_{1e,I-1,J+1} - U_{1e,I-1,J}) + C_2$

$b_5 = a_3$	$b_5 = a_3$
$b_6 = a_{13} + C_3$	$b_6 = - a_{13}$
$b_7 = a_6$	$b_7 = a_6$
$b_8 = -a_{11}U_{2e,I-1,J} + C_4$	$b_8 = a_{11}U_{2e,I-1,J+1}-U_{2e,I-1,J}) + C_5$
$b_9 = a_{11} + a_7$	$b_9 = a_{11} + a_7$
$b_{10} = -a_{12}U_{2e,I,J-1} + C_5$	$b_{10} = a_{12}\ (U_{2e,I-1,J+1} - U_{2e,I-1,J}) + C_5$
$b_{11} = a_8$	$b_{11} = a_8$
$b_{12} = -a_{11} + C_6$	$b_{12} = -a_{14}$

$$e_1 = \frac{U_{1e}}{H_1 \Delta X_{1,I-1}}$$

$$e_2 = \frac{U_{2e}}{H_2 \Delta X_{2,J-1}}$$

$e_4 = e_1 + e_2$	$e_4 = e_1$
$e_5 = e_1 I_{e,I-1,J} + e_2 I_{e,I,J-1}$	$e_5 = e_1 I_{e,I-1,J} + e_3\ (I_{e,I-1,J+1} - I_{e,I-1,J})$

where the coefficients on the left side of the page are for $U_{2e} > 0.0$ and those on the right are for $U_{2e} < 0.0$. Eqs. (3.11.17),(3.11.18),(3.11.19) are solved iteratively in a nested loops by successive substitution. The outer loop solves for the density. If the flow is incompressible, the density $\rho = 1.0$. The inner iteration loop solves for the velocity components and rothalpy. Assume U_{2e} is known, then Eq. (3.11.17) can be solved for U_{1e}. With U_{1e} known, Eq. (3.11.18) can be solved for U_{2e}. Since both equations are quadradics, they are solved in the following manner;

$$\phi_1 = (b_2 + b_3\, U_{2e})^2 - 4b_1\,(b_6 + b_4\, U_{2e} + b_5 U_{2e}^2) \qquad (3.11.20)$$

$$\phi_2 = (b_{10} + b_9\, U_{1e})^2 - 4\, b_{11}\,(b_{12} + b_8\, U_{1e} + b_7\, U_{1e}^2) \qquad (3.11.21)$$

and

$$U_{1e} = -\frac{(b_2 + b_3\, U_{2e}) + \sqrt{\phi_1}}{2\, b_1} \qquad |\, b_1| > 0 \qquad (3.11.22)$$

$$U_{2e} = -\frac{(b_{10} + b_9\, U_{ie}) + \sqrt{\phi_2}}{2\, b_{11}} \qquad |\, b_{11}| > 0$$

$$= \frac{+\, b_8\, U_{ie} + b_7\, U_{ie}^2}{b_{10} + b_9\, U_{ie}} \qquad b_{11} = 0 \qquad (3.11.23)$$

where the positive roots are appropriate. When the velocity components are known, the rothalpy is determined from Eq. (3.11.3), and the remaining roperties from Eqs. (3.11.14),(3.11.15), and (3.11.16) so that the density is updated in the outer iteration loop.

4.0 RESULTS AND DISCUSSION

4.1 Introductory Discussion

In this assessment of the applicability of three dimensional boundary layer theory to predict the flow streamlines and heat transfer in a gas turbine passage four regions of the flow field are examined. These regions are the turbine pressure surface, the turbine endwall surface, the turbine suction surface, and the rotor pressure surface as indicated by the shaded areas on Fig. 1. The first three cases test the analysis in a stationary coordinate system and the fourth in a rotating coordinate system. Experimental data for pressure, endwall, and suction surfaces were obtained by Graziani et.al. (Ref. 11) in a large gas turbine cascade which simulated a turbine rotor. Detailed wall static pressure distributions, three component velocity traverses, wall heat transfer, and wall limiting stream lines were presented. Data for the rotating blade case was obtained by Dring And Joslyn (Refs. 12 and 13). This data includes wall static pressure distributions and wall limiting streamlines. In addition, radial traverses of the total pressure and flow angle in the stationary reference frame upstream of the rotor were given. This data was sufficient to calculate the cases presented in this section.

Initial results using this three dimensional boundary layer analysis have been presented by Vatsa (Refs. 1 and 2) wherein the boundary layer edge conditions were obtained directly from the velocity traverses. In the assessment presented in this section the boundary layer edge conditions were obtained by integrating the surface Euler equations using the measured static pressure distributions. The overall analytical procedure, which was the same for all cases, is shown on the flow chart shown on Fig. 3. Spline smoothed Cartesian coordinates of the turbine blade surface are used to calculate a coordinate system using the geometry analysis presented in Section 3.10. With the coordinates known, the experimental pressure distribution was used to calculate the boundary layer edge conditions using the surface Euler analysis given in Section 3.11. Finally, the three dimensional boundary layer equations, given in Section 3.4, were solved. The inflow conditions were estimated using the local similarity approximation, described in Secton 3.7, along all inflow planes that are not characteristic surfaces. For the cascade pressure surface case, the plane of symmetry is a characteristic surface and the inflow conditions were estimated using the plane of symmetry analysis also described in Section 3.7. Integral properties of the boundary layer such as displacement thickness and momentum thickness (defined for a three dimensional boundary layer) were calculated for all cases. These integral properties of the boundary layer were obtained from the velocity vectors resolved in an intrinsic coordinate system defined by the free stream flow direction and the cross flow direction (see Appendix). In addition the two components of the wall friction coefficient (streamwise and crossflow), heat transfer (Stanton number), and wall limiting

streamline skew angles were calculated. The Stanton number was calculated in two steps. In the first step, the adiabatic wall temperature was calculated by assuming zero heat flux at the wall. In the second step, a constant heat flux equal to that applied experimentally was used, and the wall temperature calculated. Thus the calculation procedure used for determining the Stanton number was the same as that used experimentally in Ref. 11.

4.2 Turbine Cascade Pressure Surface

The turbine cascade pressure surface developes a nearly two dimensional boundary layer since the passage vortex is near the suction surface as shown on Fig. 1. Since the spanwise static pressure distributiuon is nearly consant, little spanwise flow or skewing is expected. For this reason, the primary purpose of this test case is to demonstrate a calculation started along a plane of symmetry boundary. The computational domain extends from a point just down stream from the leading edge of the turbine blade to a point just upstream of the trailing edge of the blade and spanwise from the plane of symmetry to the endwall. The coordinates calculated for this case consists of a 40 by 40 grid with 100 grid points normal to the surface grid of which every other coordinate line is plotted on Fig. 5. The calculated boundary layer edge conditions are shown on Fig. 6 in the form of velocity vectors projected on to the $Y_3 = 0.0$ plane. These velocity vectors show, as expected, very little spanwise flow at the edge of the boundary layer. Since the pressure distribution was not accurately known near the leading edge, the boundary layer calculation was started with a finite boundary layer thickness using the local similarity approximation by specifying a finite distance ($\xi_1 > 0$) for the virtual origin (see Sect. 3.7). The boundary layer was assumed to be completely turbulent throughout. A plot of the wall limiting streamlines is shown in Fig. 7 in the form of the wall stress vectors projected on to the $Y_3 = 0.0$ plane. Again this vector plot shows very little spanwise flow. In addition, the skew angle (the angle between the boundary layer edge flow direction and wall streamline direction) is not more than ten degrees. These results compare favorably with the experimental results for flow direction and flow skewing presented by Graziani et. al. in Ref. 11.

4.3 Turbine Cascade Endwall Surface

The endwall surface boundary layer has a large cross flow produced by the strong static pressure gradient from the pressure surface to the suction surface as shown in Fig. 1. In addition this boundary layer has a complex pattern produced by a separation and attachment line and a saddle point. Downstream of this region the boundary layer is rapidly accelerated and the boundary layer growth is more systematic. In this downstream region it may be possible to use three dimensional boundary layer theory. The computational domain and skewed

coordinate system used for this case is shown on Fig. 8. It consists of a 40 by 40 grid with 100 grid points normal to the surface grid which extends from a point just downstream from the saddle point to just upstream of the trailing edge to the suction surface of the blade passage. The boundary layer edge conditions were calculated using the wall static pressure distribution for the thick boundary layer case presented by Graziani et. al. (Ref. 11). Along the inflow boundaries for the surface Euler calculation, it was assumed that the boundary layer edge flow was tangent to the X_1 coordinate line so that U_{2e} was assumed zero. Integration of the surface Euler equations showed that futher downstream small negative cross flow velocities developed indicating that the boundary layer edge flow curvature was less than the coordinate curvature. This result was consistent with the velocity traverse data used by Vatsa (Refs. 1 and 2). Since this small negative U_{2e} velocity component produced stability problems (see Section 3.9) which could not be resolved even with a much finer grid, the calculation for the edge velocity conditions was run assuming that U_{2e} was zero in agreement with the procedure of Vatsa (Ref. 2). A plot of the edge velocity vectors, which are tangent to the X_1 coordinate lines, is shown on Fig. 9.

The boundary layer calculation was started with inflow conditions obtained from local similarity solutions of the boundary layer equations. A comparison of the calculated wall shear vectors with the measured surface streamlines is shown on Fig. 10. As seen in this figure, the flow inclinations are in qualitative agreement with the measured data except in the neighborhood of the saddle point. It is also noted that the calculation presented here using the measured wall static pressures to derive the boundary layer edge conditions shows much better agreement for the predicted flow angle than the calculations of Vatsa (Ref. 2) which used measured velocities for the edge conditions. This result indicates the difficulty in determining the edge of the boundary layer in a three dimensional flow field. Improved results perhaps may be obtained with better definition of the flow conditions along the upstream inflow plane. A comparison of the measured and calculated heat transfer (Stanton number) distributions is shown in Fig. 11 in the form of contour plots. Again qualitative agreement is obtained except in the region of the saddle point. The case presented by Vatsa (Ref. 1) is the same as that presented here except that the edge velocities were determined directly from three component velocity traverses whereas in the present case the edge velocities were calculated from the wall static pressure distribution using the surface Euler equations. Of interest then is a comparison of the predictions of heat transfer using the two methods. This is shown on Fig. 12 in the form of crossection plots of Stanton number vs. spanwise distance a several axial stations. Good qualitative agreement is obtained between the two methods where the difference between the results illustrates the difficulty in obtaining precise boundary layer edge conditions from measured data in a complex three dimensional flow field.

4.4 Turbine Cascade Suction Surface

The suction surface boundary layer of a gas turbine blade develops strong three dimensional effects due to the presence of the passage vortex which sweeps the flow up from the end wall surface. Since the boundary starts at the stagnation point near the leading edge of the blade, the leading edge inflow conditions are well established. However the flow from the end wall inflow surface produces a separation line which divides the midspan flow from the end wall flow. This inflow is less well established. The computational domain and coordinate system for this case is shown on Fig. 13. It consists of a 40 by 40 grid with 100 grid points normal to the surface grid extending from just downstream from the leading edge of the blade to just upstream of the trailing edge of the blade and from the end wall to the mid plane or plane of symmetry. The boundary layer edge conditions were calculated assuming zero cross flow velocities at the leading edge inflow plane. Along the endwall inflow plane, the flow angle and hence cross flow U_{2e} velocity was estimated from the measured surface streamlines given by Graziani et al. (Ref. 11). A plot of the calculated edge velocity vectors is shown on Fig. 14. Since the cascade surface is a developable surface, the vector plot is shown using arc length as coordinates. This vector plot clearly shows the effect of the passage vortex on the flow at the boundary layer edge. Since the surface Euler equations are hyperbolic equations with streamlines as the characteristic lines, this case illustrates difficulties which may be encountered as the flow approaches the plane of symmetry. The overall flow direction is from the endwall to the plane of symmetry. Therefore the flow along the plane of symmetry is a result of the calculation not an input boundary or inflow condition. Along this plane of symmetry the cross flow velocity is zero. Hence the static pressure must be such as to reduce the cross flow velocity to zero at the plane of symmetry. In general without sufficient data this may be difficult to achieve as was found in the present case near the blade trailing edge.

The three dimensional boundary layer equations were solved using local similarity inflow conditions as described in Section 3.7 and the local calculated edge conditions. Since this is a transition boundary layer, the begining and end of transition must be estimated because the present analysis lacks a transition model for three dimensional boundary layers. The begining and end of transition were obtained by calculating the quasi-two dimensional flow along the plane of symmetry using the intermittancy function of Dhawan and Narashima (Ref. 22) and comparing the results with the experimental data for heat transfer. These transition points were then held constant across the span of the blade. A comparison of the calculated wall shear vectors with the measured wall limiting streamlines is shown on Fig. 15. The flow direction at the wall is seen to be calculated quite well and the separation line separation line dividing the leading edge flow from the end wall flow is also predicted quite well. A comparison of the measured and calculated Stanton number distributions is shown on Fig. 16.

Again encouraging agreement is obtained both as to magnitude and overall pattern. The calculation, however appears to underpredict the peak heat transfer which occurs near the endwall inflow plane. Crossection plots of the Stanton number versus spanwise distance at different axial stations are shown on Fig. 17. These plots show that the average level of heat transfer across the span is predicted reasonably well, but that the high and low regions are underpredicted. Calculated and measured heat transfer along the midplane of the blade is shown on Fig. 18. This figure also shows predictions made from a two dimensional calculation using the present three dimensional boundary layer analysis and also predictions made by Sharma (Ref. 25). These comparisons show that although the flow is quasi two dimensional along the plane of symmetry (i.e. $U_{2e} = 0.0$), the heat transfer is not predicted accurately. Sharma (Ref. 25), with a quasi 3-D calculation, showed that this difference can be accounted for by the streamline convergence of the flow toward the plane of symmetry. Thus it may be expected that the difference between the calculated 3-D heat transfer and the measured heat transfer can in large part be accounted for by errors in the prediction of streamline convergence. Vatsa (Ref. 1) obtained better predictions of the heat transfer along the midplane using measured velocities for the edge conditions. Since no pressure distribution data was available from the quarter-plane to the midplane for this case, the streamline convergence of the flow towards the midplane could not be estimated by the surface Euler analysis as accurately as otherwise might be possible.

The three dimensional boundary layer analysis also calculates the wall friction coefficients and integral parameters such as displacement and momentum thickness. Since a nonorthogonal coordinate system may be rather arbitrary and not reflect the flow properties, these parameters are calculated in a locally intrinsic coordinate system (see Appendix). This locally intrinsic coordinate system is referenced to the boundary layer edge flow direction and an orthogonal cross flow flow direction. All velocities and shear stresses are locally resolved to this coordinate system. Thus two displacement thicknesses are defined. One represents the velocity defect in the streamwise direction and the other the velocity defect in the cross flow direction. Likewise the wall friction coefficients represents the wall shear in the streamwise and cross flow direction. Contour plots of the streamwise component of wall friction coefficient and displacement thickness are shown on Figs. 19 and 20.

4.5 Turbine Rotor Pressure Surface

The flow over the rotor pressure surface is strongly influenced by the relative vorticity generated by rotation of coordinates. Thus the boundary layer flow is driven by two applied forces; the pressure gradient, and the Coriolis force. Because of rotation rotation, the pressure surface sees a strong radial pressure gradient which tends to drive the flow radially inward. The Coriolis

force may tend to drive the flow radially inward or outward depending on the sign of the blade rotation vector normal to the surface Ω_3. The balance of these forces tends to drive the flow radially outward near the leading edge and axially near the trailing edge. The computational domain and coordinate grid for this problem is shown on Fig. 21. It consists of a 40 by 40 grid with 100 grid points normal to the surface grid extending from just downstream from the leading edge stagnation line to just upstream of the trailing edge and from the rotor hub to the rotor tip. The boundary layer edge velocity vectors calculated from the surface Euler equations are shown on Fig. 22. It was found that no solution of the surface Euler equations exist along the leading edge inflow boundary for the crossflow velocity $U_{2e} = 0.0$. Therefore on both the leading edge and hub inflow boundaries, the crossflow velocity was estimated from the surface streamlines given by Dring and Joslyn (Refs. 12 and 13). The edge velocities show the behavior of the suction surface flow observed by Dring and Joslyn.

The boundary layer equations were started with local similarity inflow conditions. A comparison of the calculated wall stress vectors with the wall streamlines obtained using the ammonia-ozalid process is shown on Fig. 23. The calculated vectors clearly show the general overall flow pattern quite well. Calculated flow angles are compared with the flow angles measured from the ozalid paper on Fig. 24. Two curves are shown. The first curve (solid line) is the calculated flow angle at each point along the calculated streamline. The second curve (dotted line) is the calculated flow angle along the midplane. A comparison of the edge velocity vectors with the wall vectors indicates that the flow skewing is up to about ten degrees. These figures clearly show that the flow streamlines are predicted fairly accurately and that two dimensional boundary layer theory applied in a strip fashion would not be adequate to calculate the heat transfer on the turbine blade. Calculated Stanton number distributions for a fully turbulent boundary layer are shown on Fig. 25. This shows higher heat transfer rates near the hub and trailing edge of the rotor blade.

5.0 CONCLUDING REMARKS

An assessment has been made of the applicability of a three dimensional boundary layer analysis for the calculation of heat transfer, total pressure loss, and streamline flow patterns on the surfaces of both stationary and rotating turbine passages. On the pressure and suction surface of a turbine cascade, the 3-D boundary layer analysis along with the coordinate generator and surface Euler analysis produce predictions of heat transfer and surface streamline patterns which are in reasonably good agreement with available experimental data. Experimental data for wall friction coefficient was not availble to evaluate the prediction of loss; however, because of the close relation between wall friction and heat transfer one may also expect good predictions of loss. Assessment of the 3-D boundary layer analysis for the predictions of the flow on a turbine endwall is complicated by the uncertainty in the inflow conditions downstream from the separation and attachment lines. However the results obtained in this study are very encouraging as they indicate that the 3-D boundary layer analysis is applicable to the endwall surface as well. On the pressure surface of a rotating turbine blade, prediction of the flow streamlines and flow skewing agree reasonably well with the available data. Evaluation of the analysis for the prediction of heat transfer and loss on a rotating turbine blade must await the collection of experimental data.

The results obtained in this investigation reinforce earlier conclusions that two dimensional boundary layer theory applied in a strip fashion can not predict heat transfer and loss because of the strong three dimensional flow effects on a turbine blade. On the suction surface of a blade, these three dimensional effects are produced by the passage vortex and on the pressure surface of a rotating blade these effects are produced by the radial pressure gradient and Coriolis force. In view of the current state of Navier-Stokes analysis, three dimensional boundary layer theory could provide a useful tool for local enhancement of of the flow field for the prediction of heat transfer, loss, and flow streamline pattern on turbine blade surfaces. The results of this study strongly indicate that the local details of the flow field on the turbine blade surface can be accurately calculated using a two step procedure. First the overall flow field can be calculated on a coarse grid using a Navier-Stokes or parabolized Navier-Stokes analysis. Second the three dimensional boundary layer analysis can be used for local enhancement to provide details of the flow field on a much finer grid.

6.0 ACKNOWLEDGEMENT

The author wishes to acknowledge the contributions of Dr. V. Vatsa of NASA Langley Research Center and Dr. J. Carter and B. Caplin of UTRC. In addition, the author wishes to note that development of computer codes to plot results of the boundary layer analysis were the result of independent research activities at UTRC.

7.0 REFERENCES

1. Vatsa, V. N.: A Three-Dimensional Boundary-Layer Analysis Including Heat Transfer and Blade Rotation Effects, Paper presented at the Third Symposium on Numerical and Physical Aspects of Aerodynamic Flows, Long Beach California, January 1985.

2. Vatsa, V. N.: A Three Dimensional Boundary Layer Analysis for Turbomachinery Applications, UTRC Report No. 84-44, 1984.

3. Howarth, L. : The Boundary Layer in Three-dimensional Flow Along a General Three Dimensional Surface, Phil. Mag. Series 7, Vol. 42 p 239 - 243 1951.

4. Squire, L. C. : The Three-Dimensional Boundary Layer Equations and Some Power Series Solutions, ARC Tech. Rpt. R&M 3006 1957.

5. Gordon, J. W. and Thiel, L. C.: Transfinite Mappings and Their Application to Grid Generation, Numerical Grid Generation, F. Thompson Ed., Elsevier Science Publishing Co. Inc. 1982.

6. Mager, A.: Three Dimensional Laminar Boundary Layers, High Speed Aerodynamics and Jet Propulsion, Ed. by F. K. Moore, Vol. IV, Princton University Press, Princton New Jersy 1964 p. 286 - 394.

7. Cebeci, T., K. Kaups, and J. A. Ramsey: A General Method For Calculating Three Dimensional Compressible Laminar and Turbulent Boundary Layers on Arbitrary Wings, NASA CR-2777, January 1977.

8. Gleyzes, C., and J. Cousteix: Calculation of Streamlines from Wall Pressures on a Fusiform Body, Rech. Aerosp. 1984-3.

9. Blottner, F. G.: Finite difference Method of solution of the Boundary Layer Equations, AIAA Journal, Vol. 18, p. 193-205 February 1970.

10. Werle, M. J. and J. M. Verdon: Viscid/inviscid Interaction Analysis for Symmetric Trailing Edges, UTRC Report R79-914493-5 January 1980.

11. Graziani, R. A., Blair, M. F., Taylor, J. R. and Mayle, R. D.: An Experimental Study of Endwall and Airfoil Surface Heat Transfer in a Large Scale Turbine Blade Cascade, Trans. ASME, J. of Eng. for Power, Vol. 102, No. 2, April 1980, p. 257-267.

12. Dring, R. P., and Joslyn, H. D.: Measurements of Turbine Rotor Blade Flows, Trans. ASME J. of Eng. for Power, Vol 103, No. 2, April 1981, p. 400-405.

13. Dring, R. P. and H. D. Joslyn: The Relative Eddy in Axial Turbine Rotor Passages, ASME paper 83-GT-22, 1983.

14. Warsi, Z. U. A.: Tensor and Differential Geometry Applied to Analytic and Numerical Coordinate Generation, Mississippi State University Report MSSU-EIRS-81-1, December 1980.

15. Bradshaw, P.: Effects of Streamline Curvature on Turbulent Flow, AGARDograph No. 169, August 1973.

16. Blottner, F. G.: Computational Techniques for Boundary Layers AGARD Lecture Series 73, presented at VKI, February 1975.

17. Vatsa, V. N. and Davis, R. T.: The Use of Levy-Lees Variables in 3-D Boundary Layer Flows. NASA CR-112315, January, 1973.

18. Wang, K. C.: On the Determination of the Zones of Influence and Dependence for the Three dimensional Boundary Layer Equations, J. Fluid Mech. Vol. 8 , 1971, p. 397 - 404.

19. Blottner, F. G. and Ellis, M. A.: Finite Difference Solution of the Incompressible Three - Dimensional Boundary Layer Equations for a Blunt Body, Int. J. of Computers and Fuids Vol. 1, 1973 p. 133 - 158.

20. Cebeci, T. and Smith, A. M. O.; Analysis of Turbulent Boundary Layers, Academic Press, New York, 1974.

21. Mellor, G. L. and Herring, H. J.: Simple Eddy Viscosity Relations for Three Dimensional Turbulent Boundary Layers, AIAA J., Vol. 15 No. 6, 1977, p 886 - 887.

22. Dhawan, S. and Narasimha, R.: Some Properties of Boundary Layer Flow During Transition from Laminar to turbulent Motion, J. of Fluid Mechanics, Vol 3, 1958, p. 418-436.

23. McCartin, B. J. : Theory,Computation,and Application of Exponential Splines, Courant Mathematics and Computing Laboritories,October 1981.

24. Spath, H. : Spline Algorithms for Curves and Surfaces, Utilitas Mathematica Publishing Co. Inc., Winnipeg, 1974

25. Sharma, O. P., and Graziani, R. A.: Influence of Endwall Flow on Airfoil Suction Surface Midheight Boundary Layer Development in a Turbine Cascade, Trans. ASME J. of Eng. for Power, Vol 105 January 1983, p 147-155

26. Anderson, O. L. and B. Caplin: User's Manual for Three Dimensional Boundary Layer Code, UTRC Report R85-956834-1, March 1985.

8.0 LIST OF SYMBOLS

a_n, c_n	Coefficients of boundary edge equations	
A_n, K_n	Coefficients of boundary layer equations	
c_p, c_v	Specific heats	
C_f	Wall friction coefficient	
C_p	Pressure coefficient	
$\vec{e}_i$	Unit vectors Cartesian coordinates	
F	X_2 velocity ratio	(u_1/u_{1e})
g_{ij}, G_{ij}	Covarient metric tensor components	(g_{ij}/ℓ^2)
G	X velocity ratio	(u_2/u_{ref})
h, H	Metric scale coefficients	(h_i/ℓ)
h , H	Static enthalpy	(h/u_∞^2)
h_T, H_T	Total enthalpy	(h_T/u_∞^2)
H	Total enthalpy ratio	(h_T/h_{Te})
i , I	Rothalpy	(i/u_∞^2)
k	Thermal conductivity	
ℓ	Reference length	
L	Levy - Lees parameter	$(\rho\mu/\rho_e\mu_e)$
M	Mach number	
$\vec{n}_i$	Unit vectors surface coordinates	
p , P	Static pressure	$(p/p_\infty u_\infty^2)$

P_T, P_T	Total pressure	$(p_T/p_\infty u_\infty^2)$
Pr, Pr_t	Prandtl number laminar/turbulent	$(c_p\ \mu/k)$
q	Levy - Lees length scale parameter	
$\dot{q}$	Heat flux	
r , R	Radius	(r/ℓ)
Re	Reynolds number	$(\rho_\infty u_\infty l/\mu_{ref})$
$\mathscr{R}$	Gas constant	
s_i, S_i	Arc length distance	(s_i/ℓ)
S_t	Stanton number	
t , T	Static temperature	(t/t_{ref})
u_i, U_i	Velocity components surface coor.	(u_i/u_∞)
u_z, U_z	Axial velocity	(u_z/u_∞)
u_r, U_r	Radial velocity	(u_r/u_∞)
u_ϕ, U_ϕ	Tangential velocity	(u_ϕ/u_∞)
u_{ref} U_{ref}	X_2 reference velocity u_{ie} or u_{2e}	(u_{ref}/u_∞)
v_i, V_i	Velocity components Cartesian coor.	(v_i/u_∞)
V	X_3 reduced velocity	
v_B, V_B	Rotor velocity	(v_B/u_∞)
x_i, X_i	Surface coordinates	(x_i/ℓ)
y_i, Y_i	Cartesian coordinates	(y_i/ℓ)
β_1	Relative inlet flow angle	
γ	Ratio of specific heats	

γ_{ij}	Direction cosine tensor components	
γ_{ij}^{-1}	Inverse tensor components	
δ	Displacement thickness	
ε	Eddy viscosity	
$\bar{\varepsilon}$	Viscosity ratio turbulent/laminar	
$\bar{\varepsilon}_{ref}$	Reference viscosity ratio	
θ	Momentum thickness	
Θ	Static temperature ratio	(t/t_{ref})
μ	Molecular viscosity	
μ_{ref}	Reference molecular viscosity	$\mu(t_{ref})$
ξ_i	Levy - Lees transformed coordinates	
ρ, ρ	Density	(ρ/ρ_∞)
τ	Time	
τ_{ij}	Stress components	
ω, Ω	Rotor speed	$(\omega\ell/u_\infty)$

Subscripts

c	Cross flow direction
e	Edge conditions
h	Hub
L	rotor inlet conditions
S	Streamwise direction
t	Tip
T	Total or stagnation conditions
∞	Free stream or reference conditions

Superscripts

~	Absolute rotor reference frame

Tensor Notation

i,j,k	Subscripts covarient tensor components
i,j,k	Superscripts contravarient tensor components

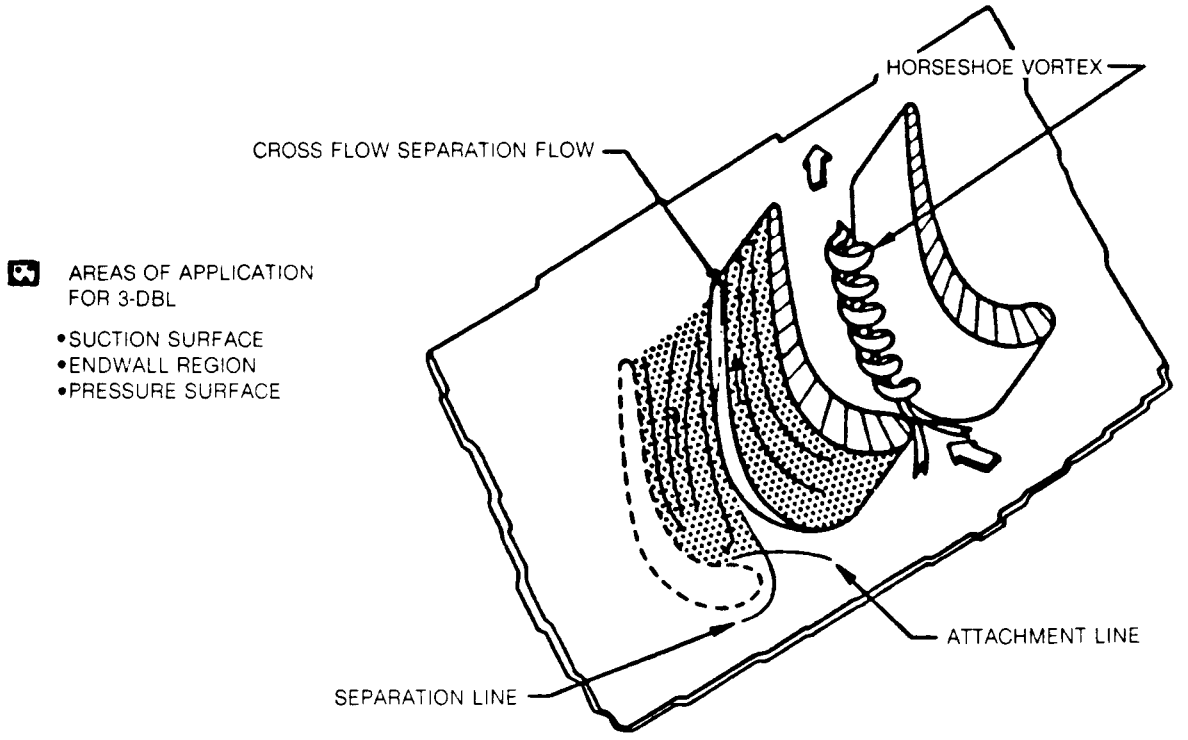

Fig. 1 Flow in a Turbine Passage

84–12–33–7

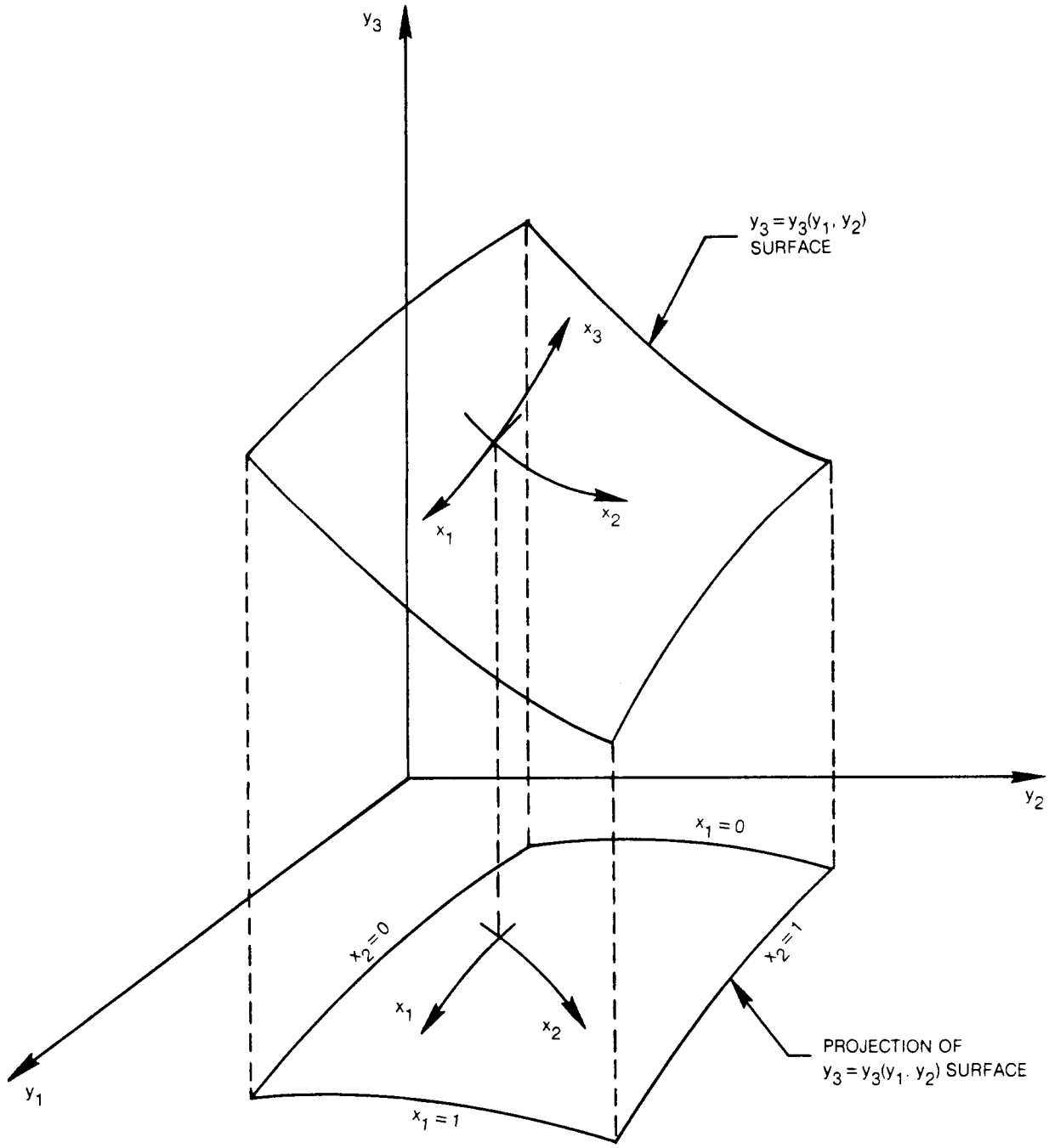

Fig. 2 Arbitrary Surface Coordinates

84-5-83-1

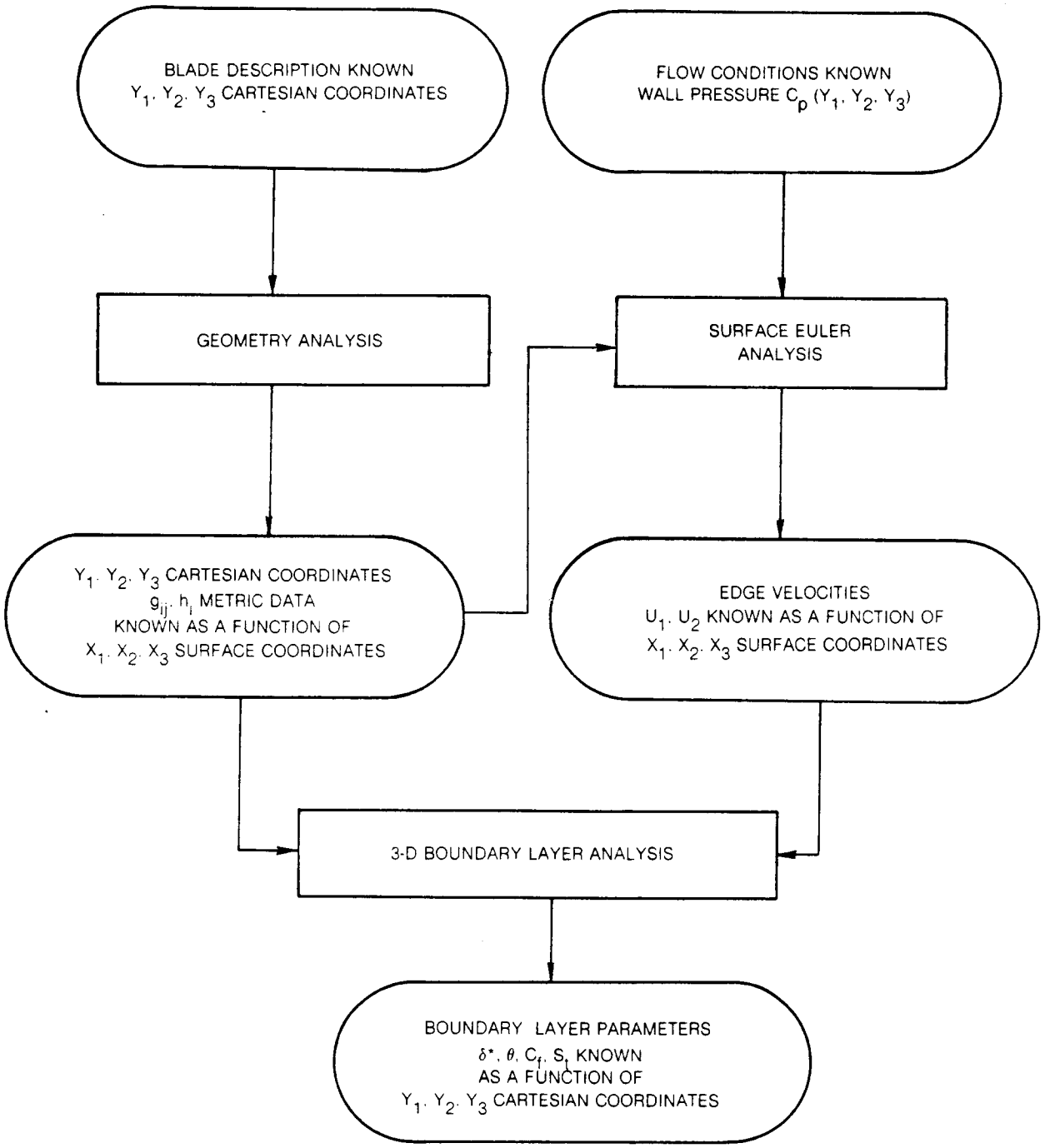

Fig. 3 Flow Chart of Geometry, Surface Euler and 3-D Boundary Layer Analysis

84–5–103–1

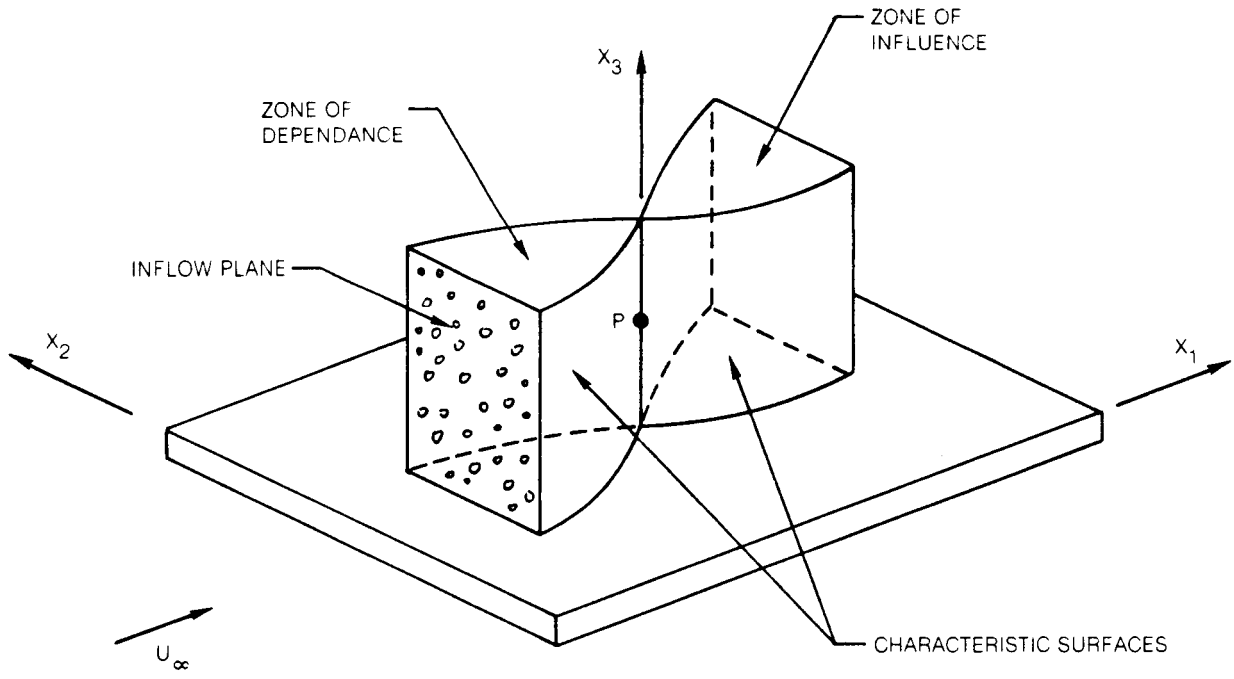

Fig. 4 Zone of Influence and Zone of Dependance for Three Dimensional Boundary Layers

85–1–87–12

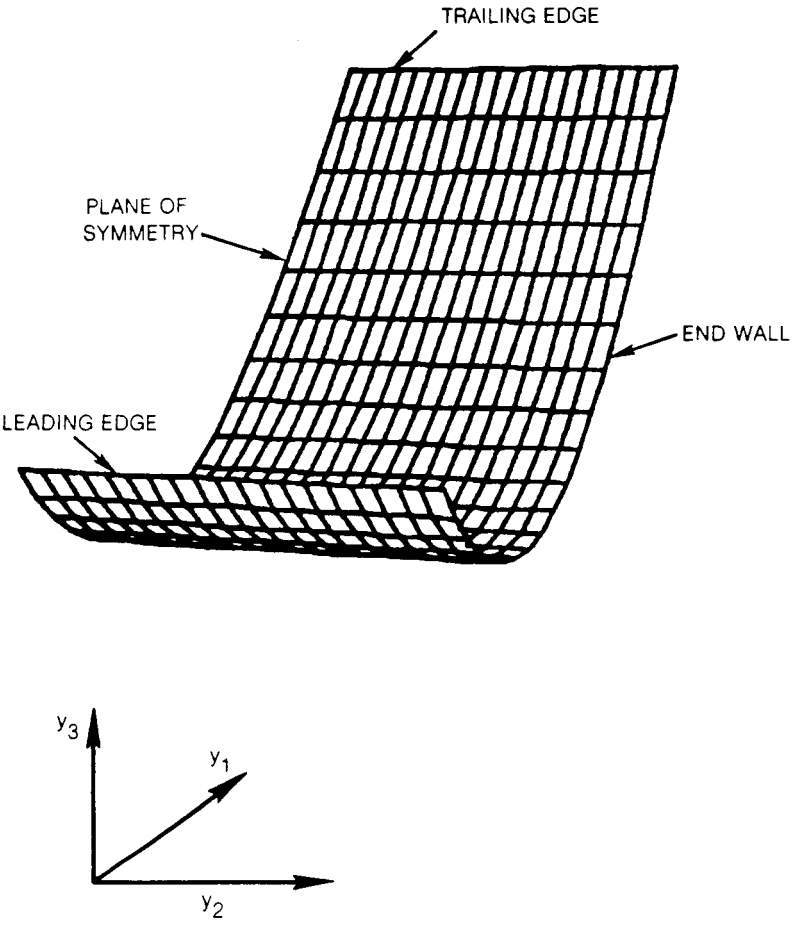

Fig. 5 Coordinate System Calculated for Cascade Pressure Surface

84-5-84-1

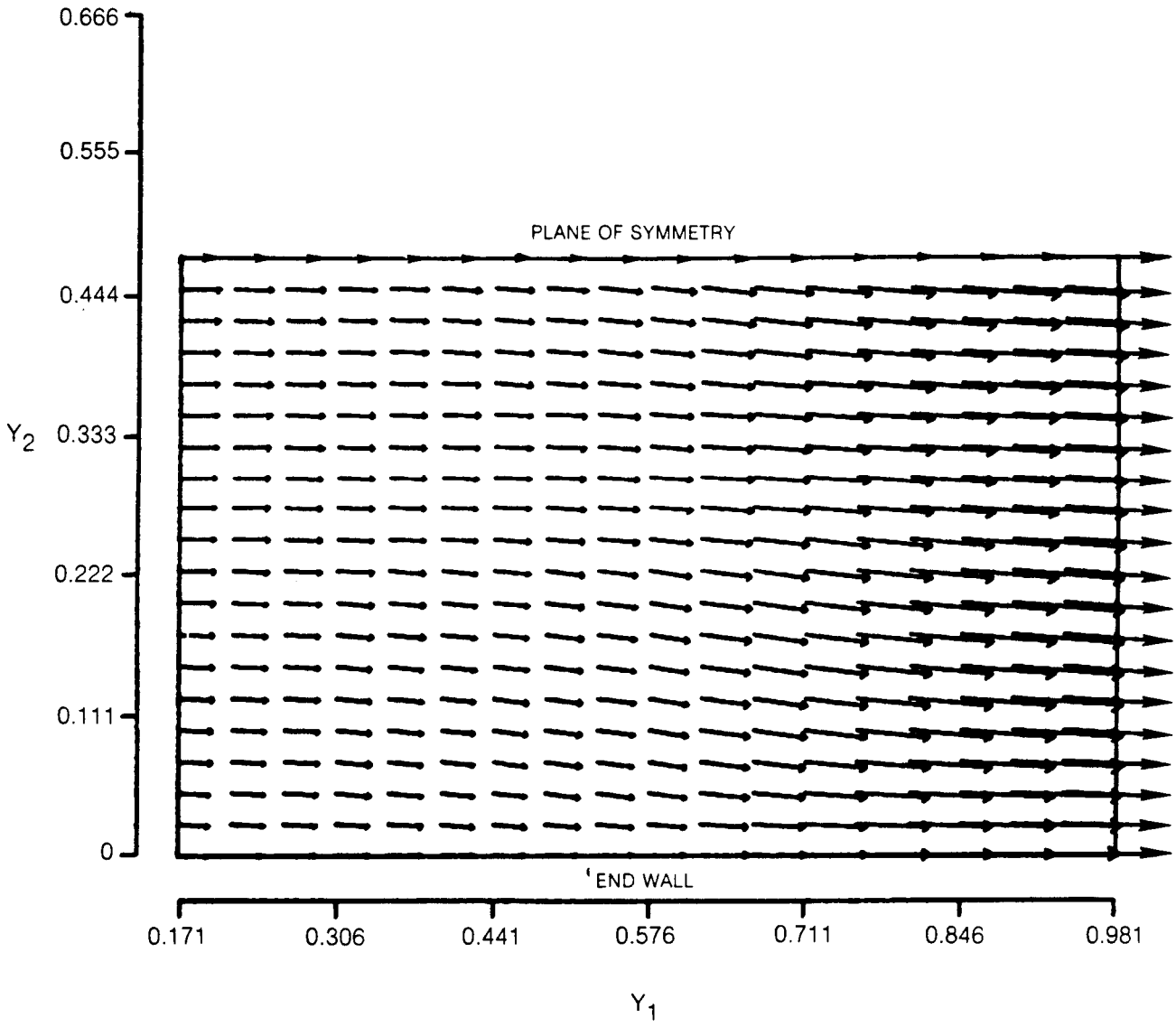

Fig. 6 Boundary Layer Edge Velocity Vectors Projected on Y_3 Plane Calculated from Experimental Static Pressure Distribution for the Cascade Pressure Surface

84-5-84-2

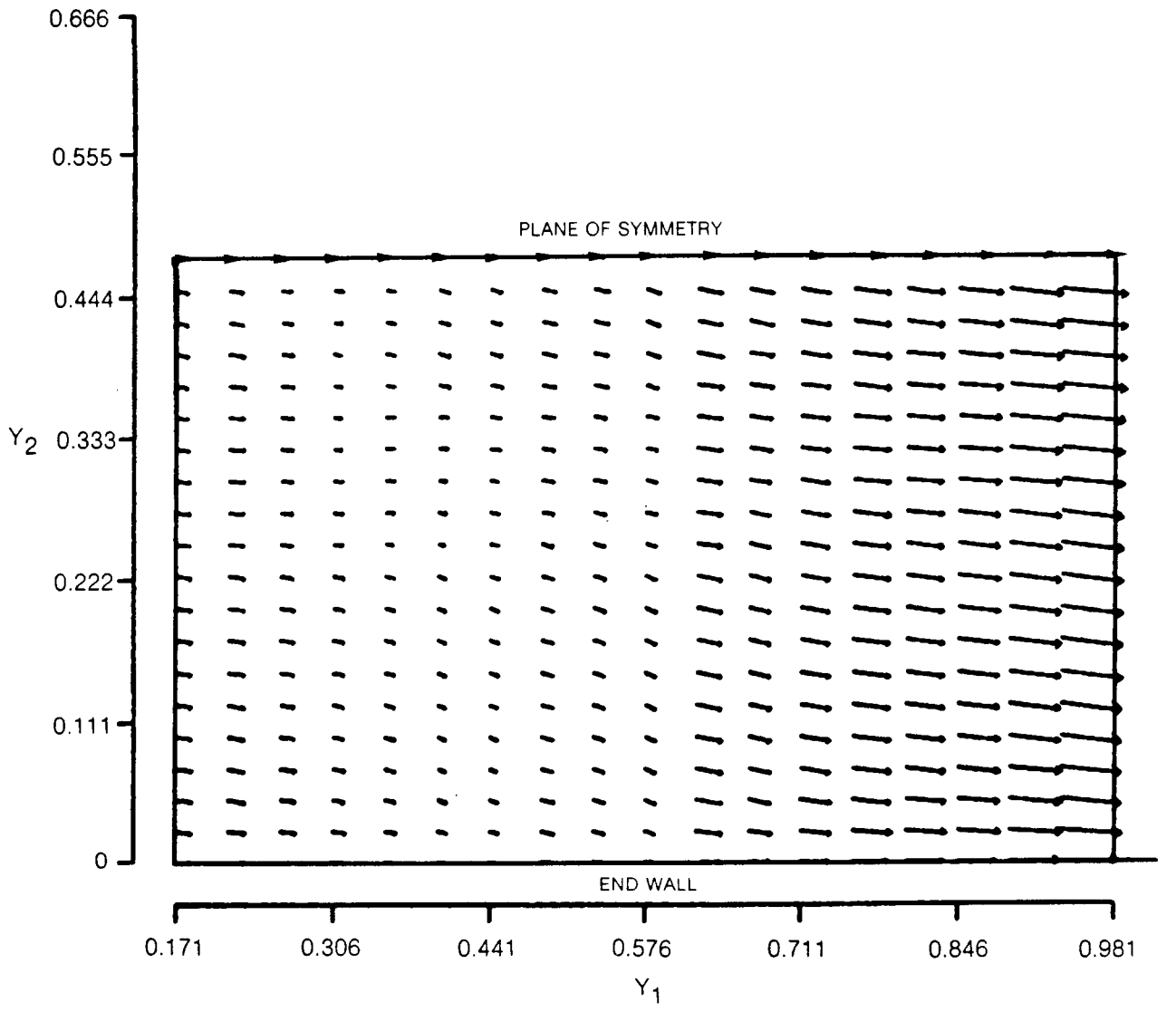

Fig. 7 Boundary Layer Wall Shear Vectors Projected on Y_3 Plane Calculated with the 3-Dimensional Boundary Layer Analysis for the Cascade Pressure Surface

84–5–84–3

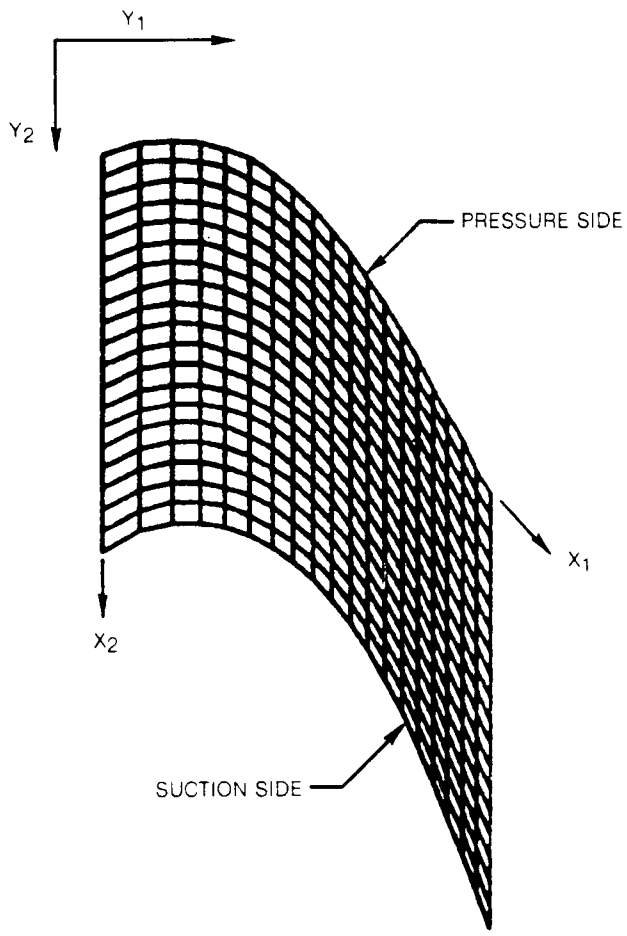

Fig. 8 Coordinate System for Cascade Endwall Surface

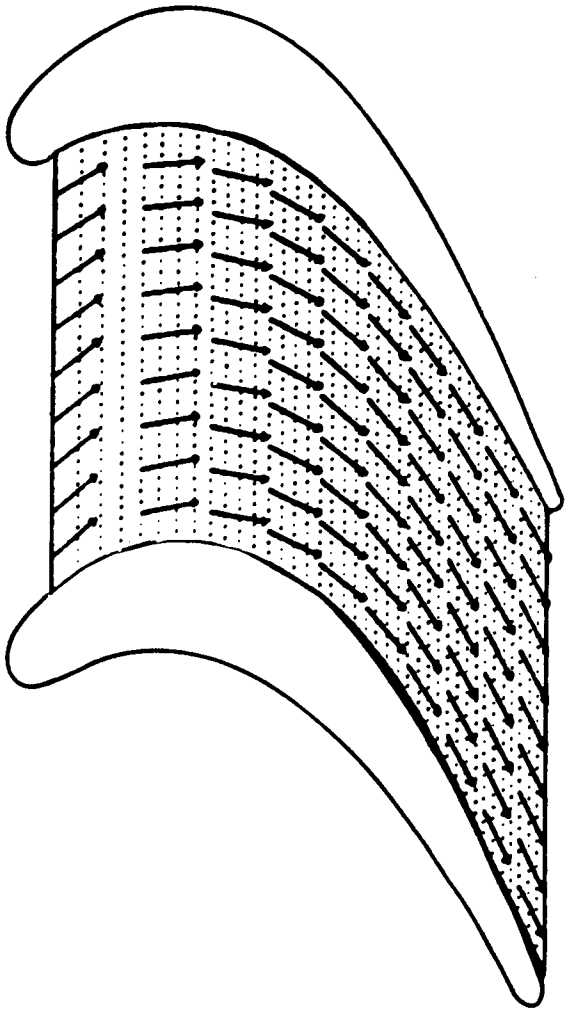

Fig. 9 Boundary Layer Edge Velocity Vectors Calculated from Experimental Surface Pressure Distributions for Cascade Endwall Surface

1.5 in. INLET BOUNDARY LAYER

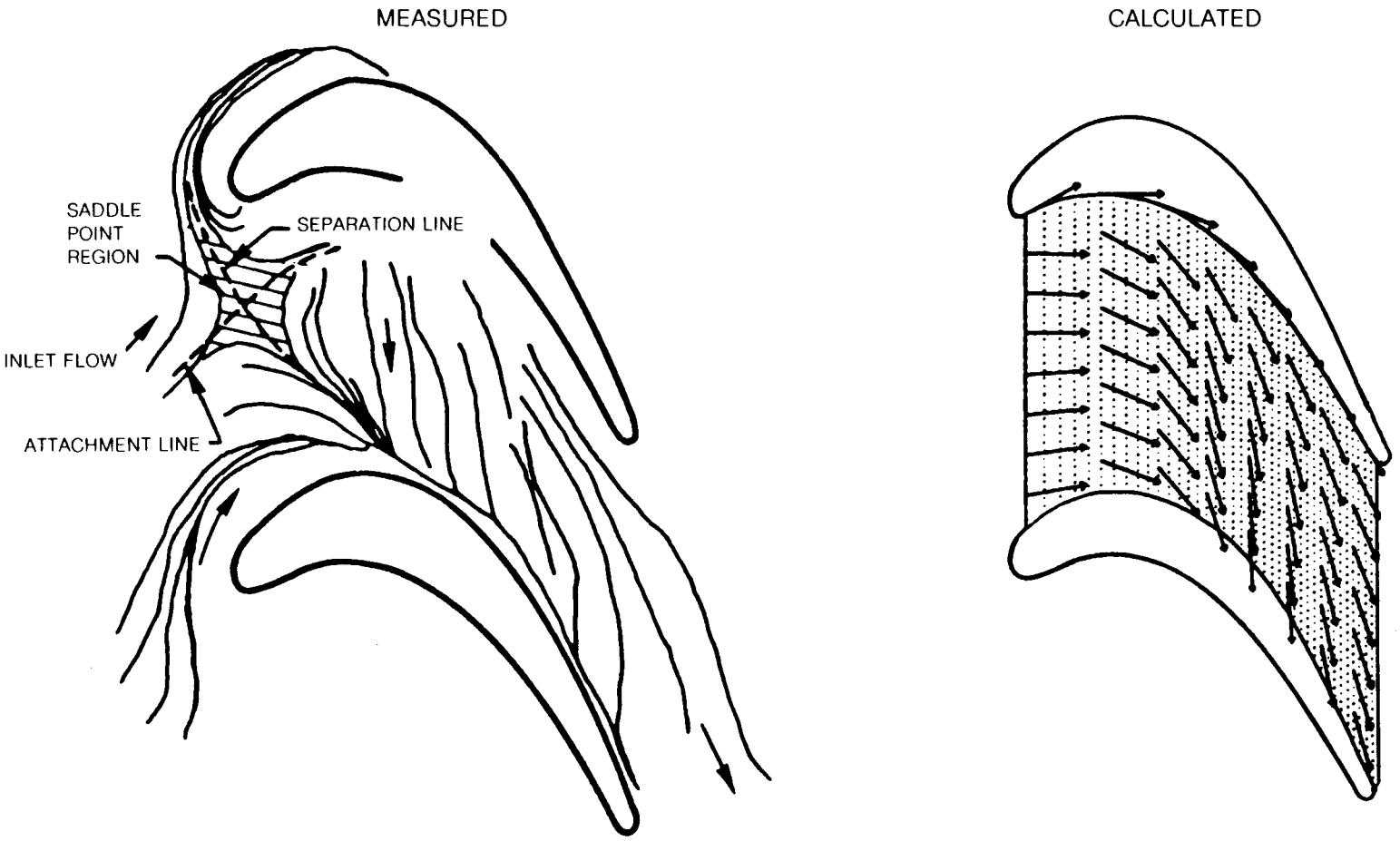

Fig. 10 Comparison of Measured and Calculated Endwall Limiting Streamlines

$$S_t = \frac{\dot{q}_w}{\rho_\infty u_\infty C_p (t_a - t_w)}$$

1.5 in. INLET BOUNDARY LAYER

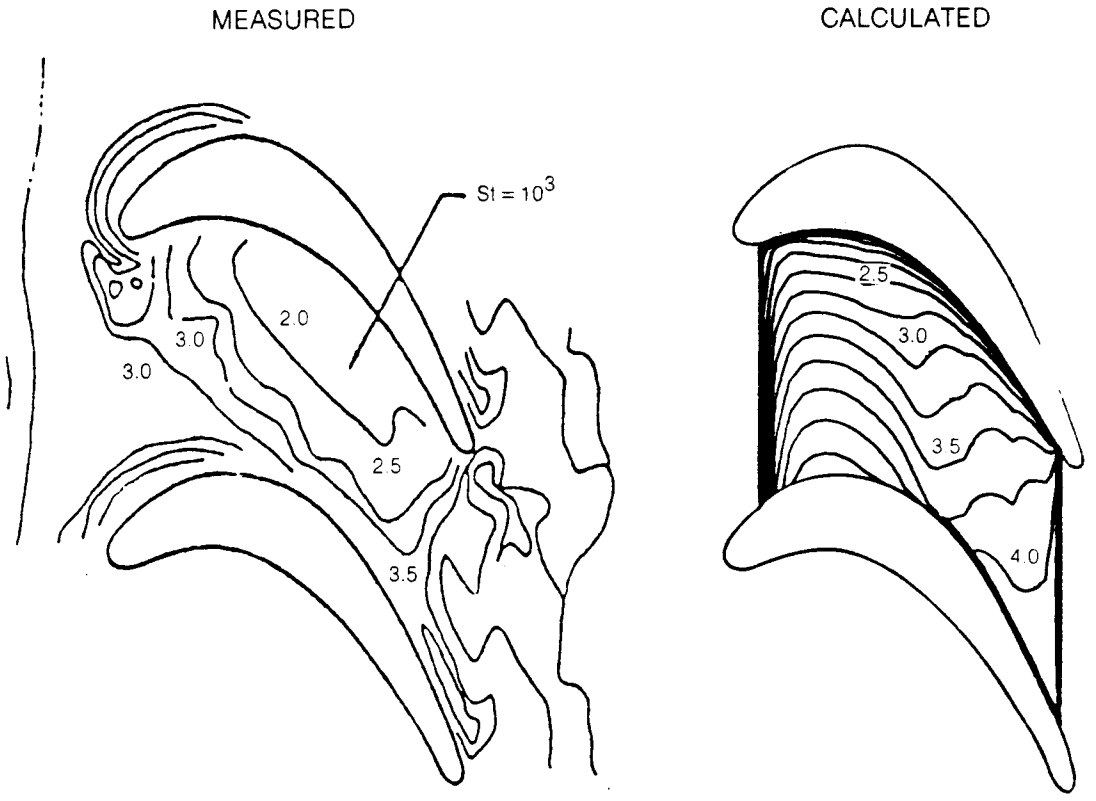

Fig. 11 Comparison of Measured and Calculated Stanton Number Distributions for End Wall Surface

85–1–87–1

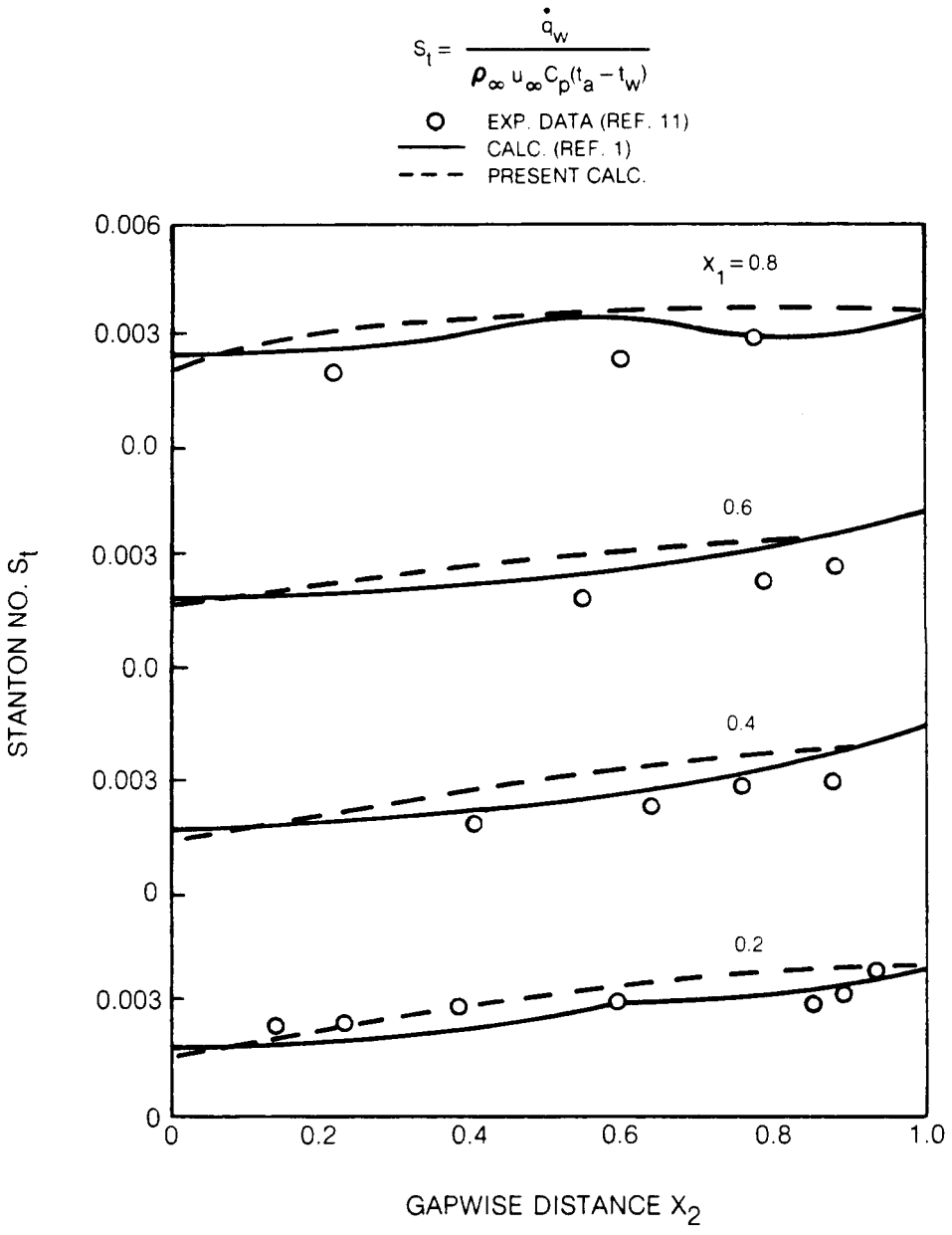

Fig. 12 Comparison of Stanton Number Distributions on Endwall Surface

85–1–87–3

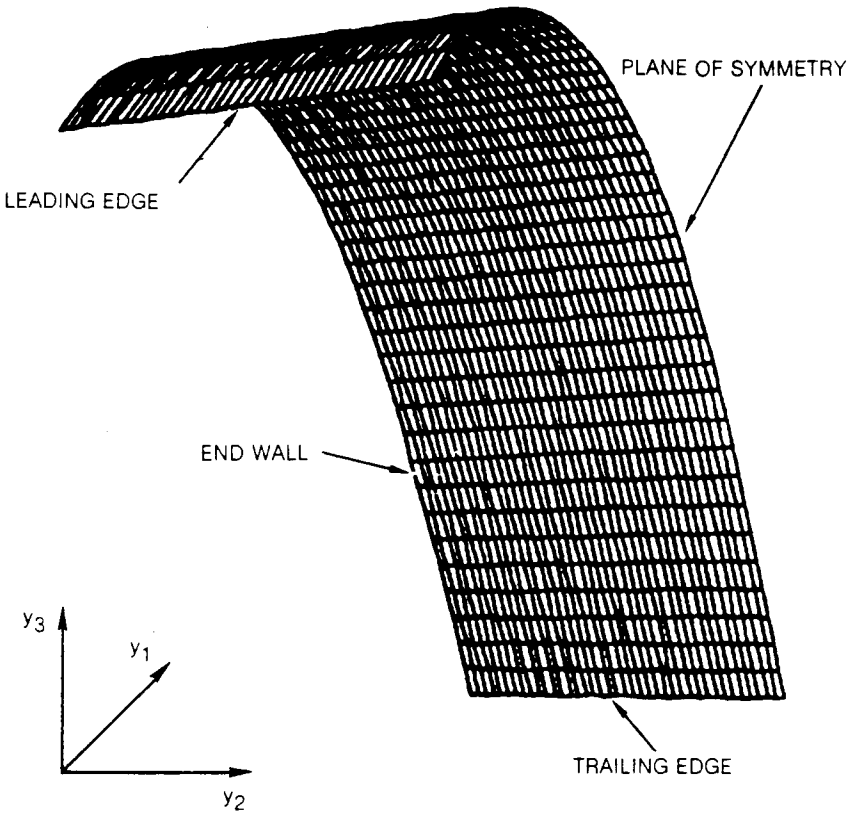

Fig. 13 Coordinate System Calculated for Cascade Suction Surface

84–7–33–1

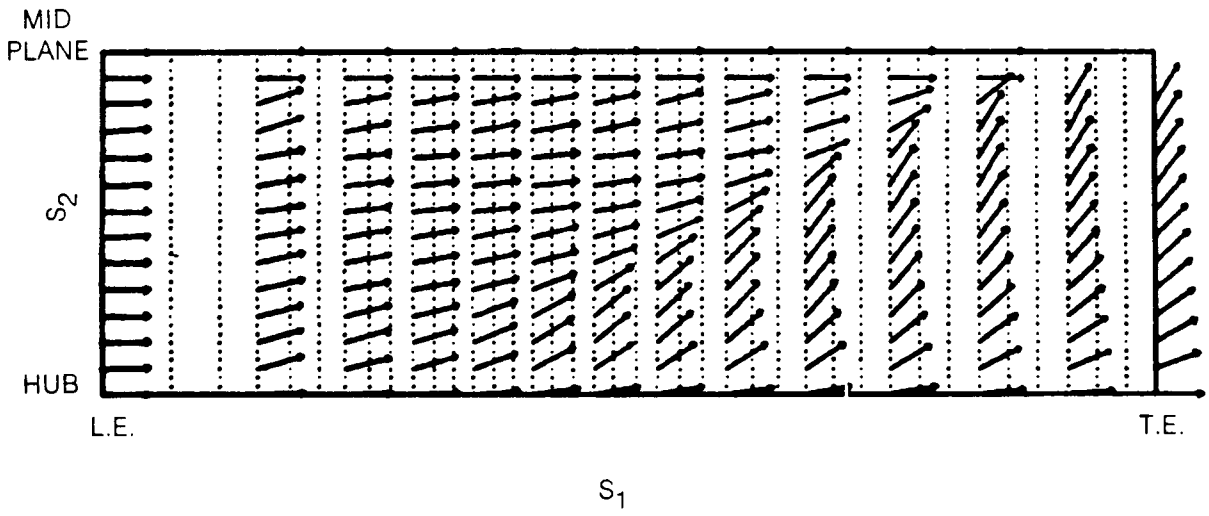

Fig. 14 Boundary Layer Edge Velocity Vectors Calculated from Experimental Surface Pressure Distribution for Cascade Suction Surface

84-12-33-1

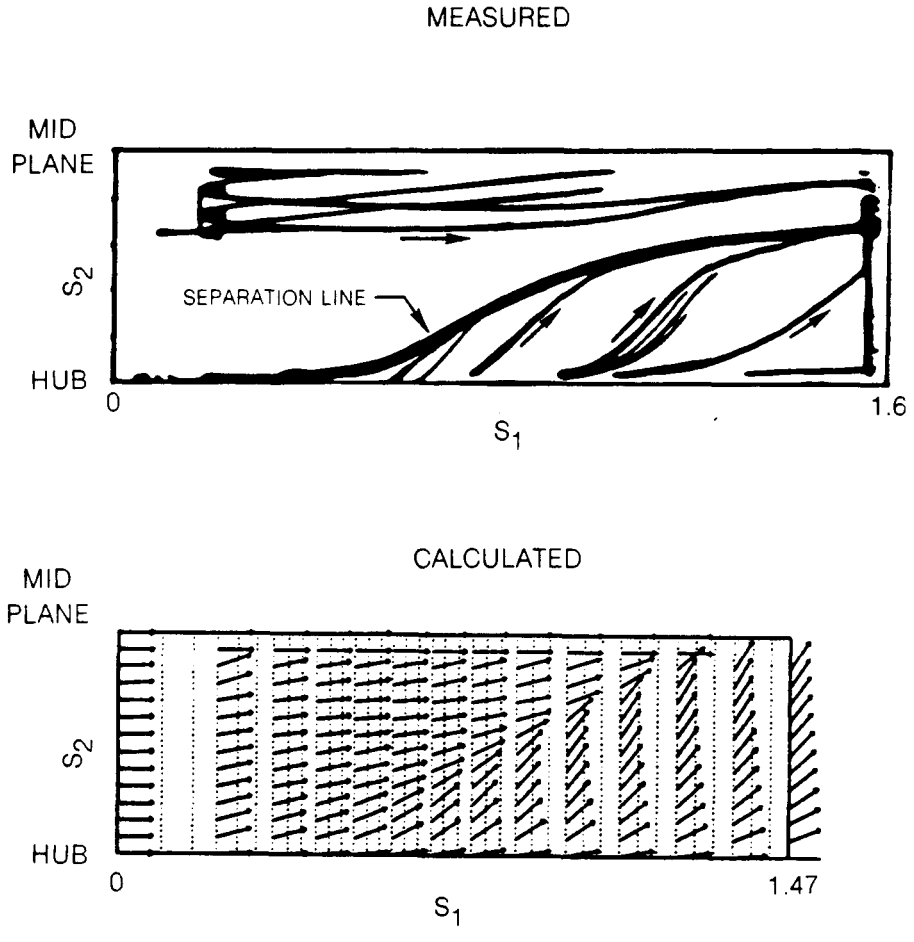

Fig. 15 Measured and Calculated Wall Limiting Streamline on Cascade Suction Surface

84-12-33-4

$$S_t = \frac{\dot{q}_w}{\rho_\infty u_\infty C_p (t_a - t_w)}$$

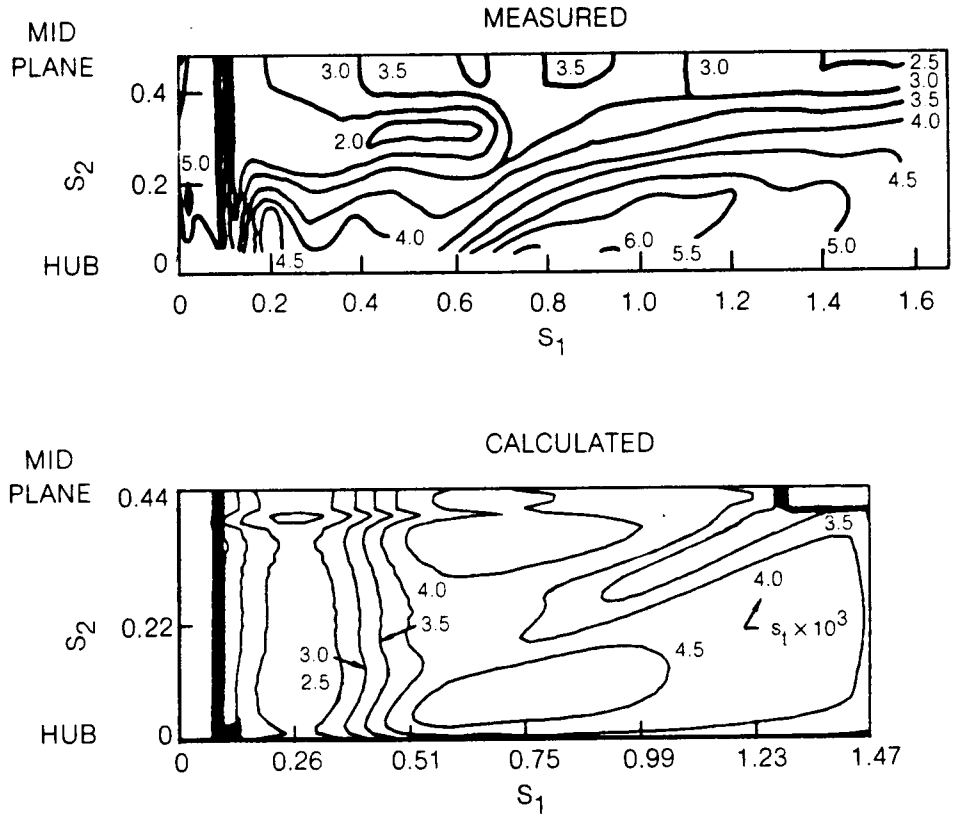

Fig. 16 Measured and Calculated Stanton Number on Cascade Suction Surface

84–12–33–5

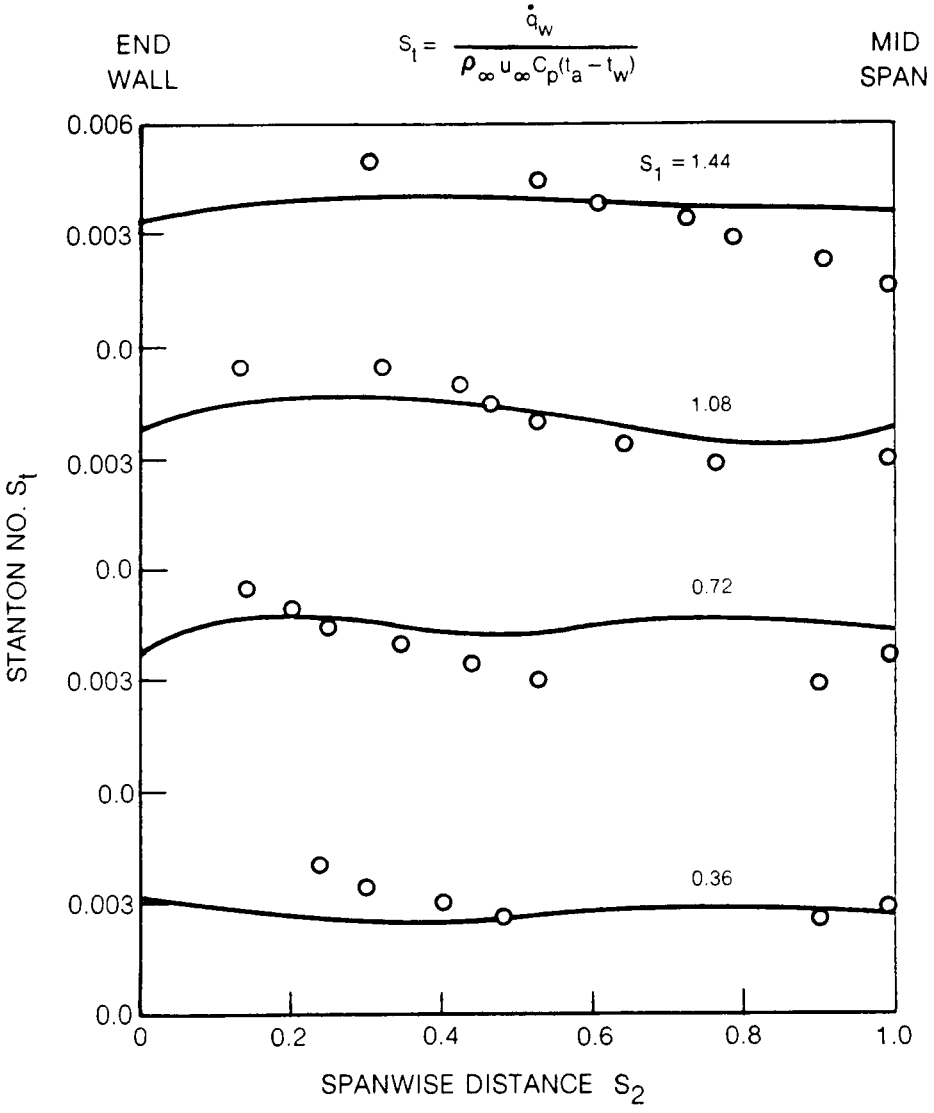

Fig. 17 Comparison of Stanton Number Distributions on Cascade Suction Surface

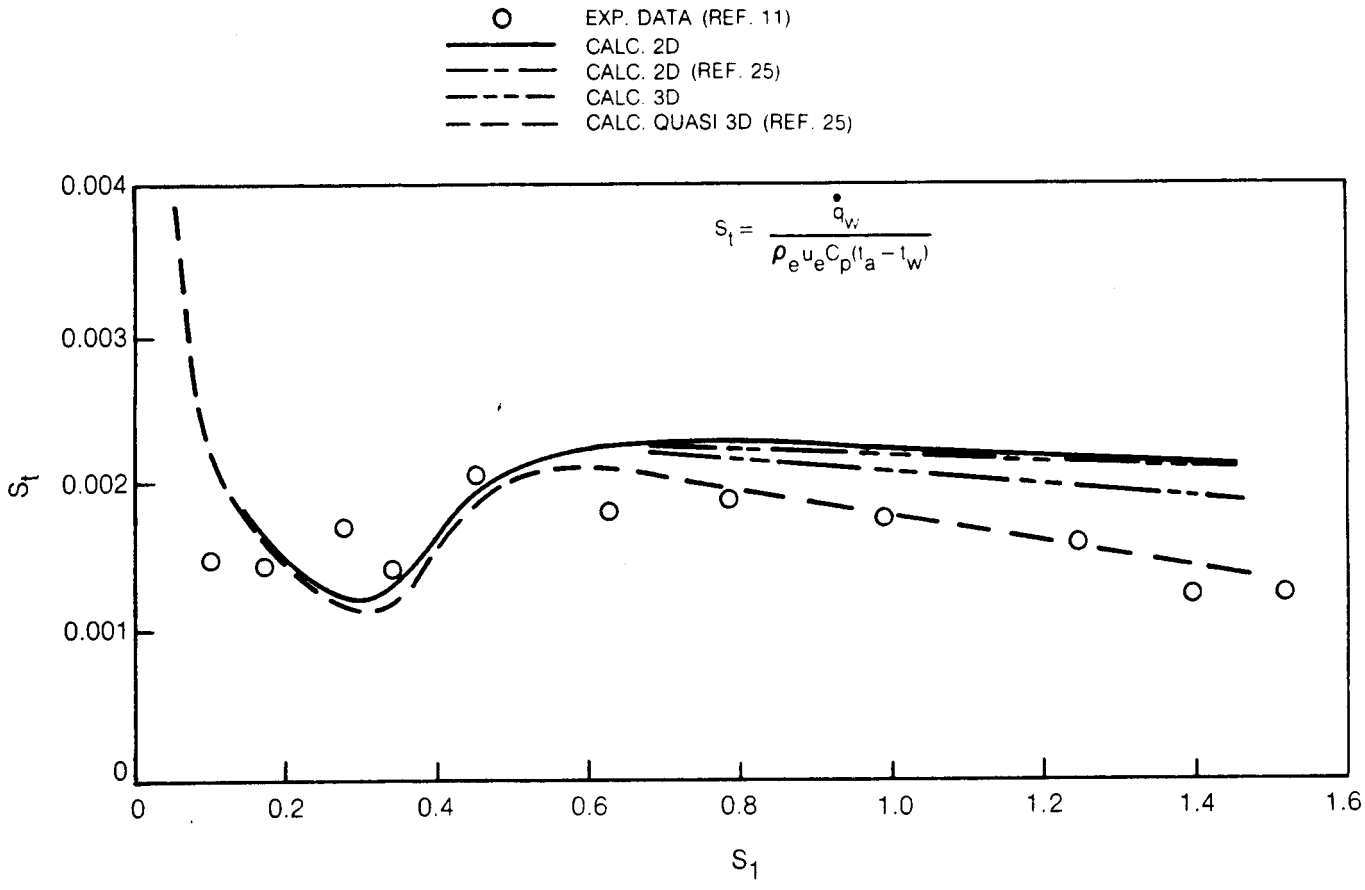

Fig. 18 Calculated and Measured Stanton Number on Mid Plane of Cascade Suction Surface

84–12–33–2

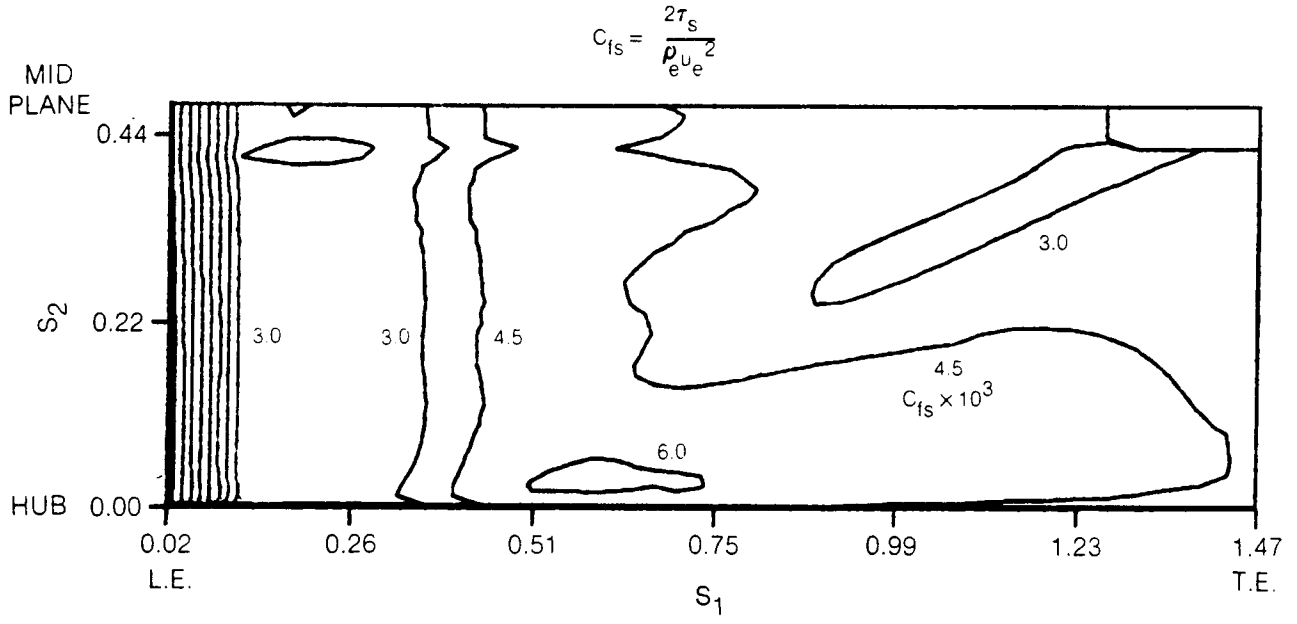

Fig. 19 Streamwise Component of Wall Friction Coefficient on Cascade Suction Surface

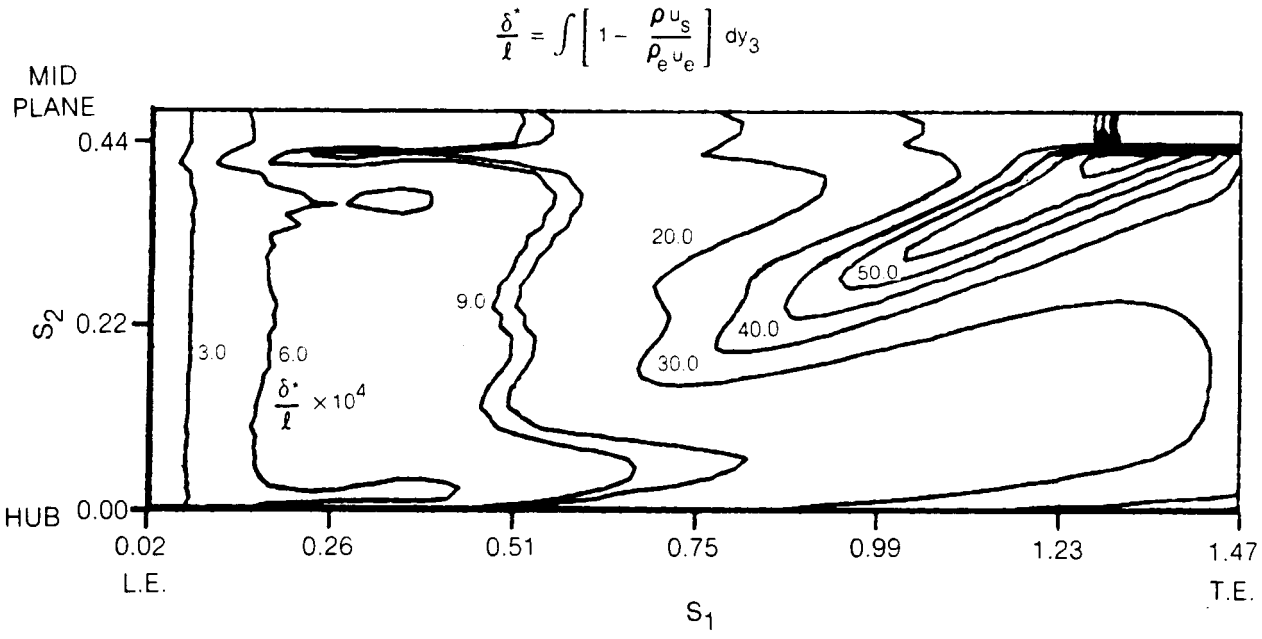

Fig. 20 Streamwise Component of Displacement Thickness on Cascade Suction Surface

85–1–87–5

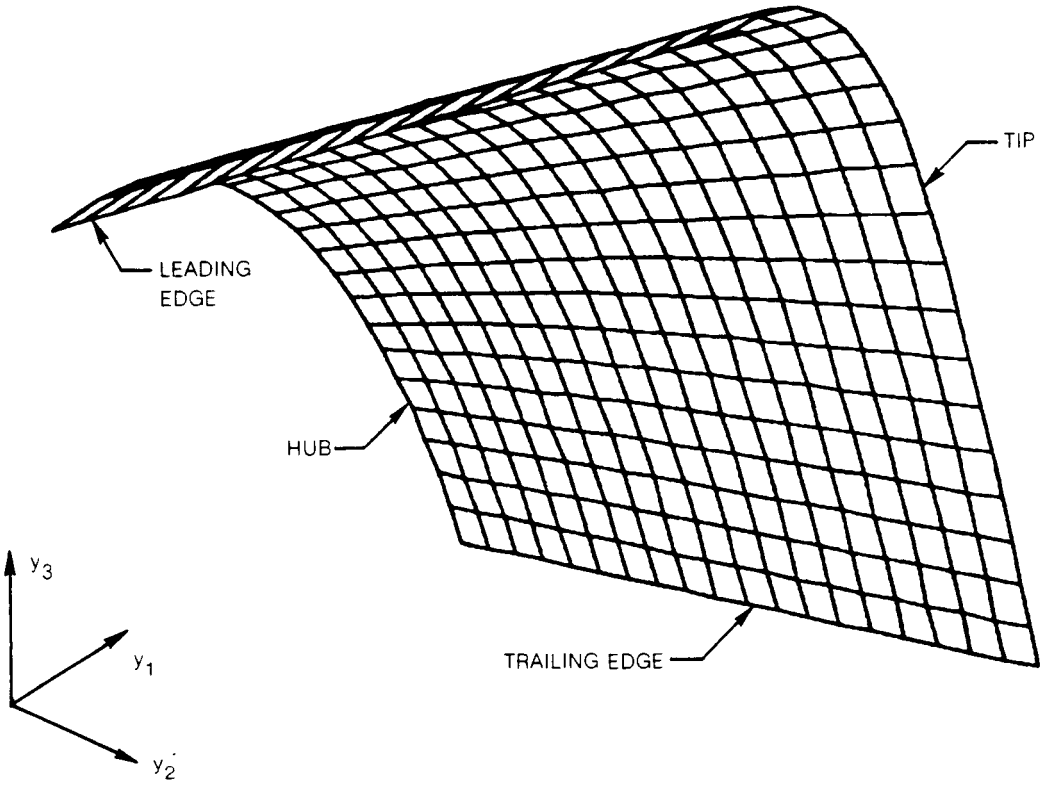

Fig. 21 Coordinate System Calculated for Turbine Rotor Pressure Surface

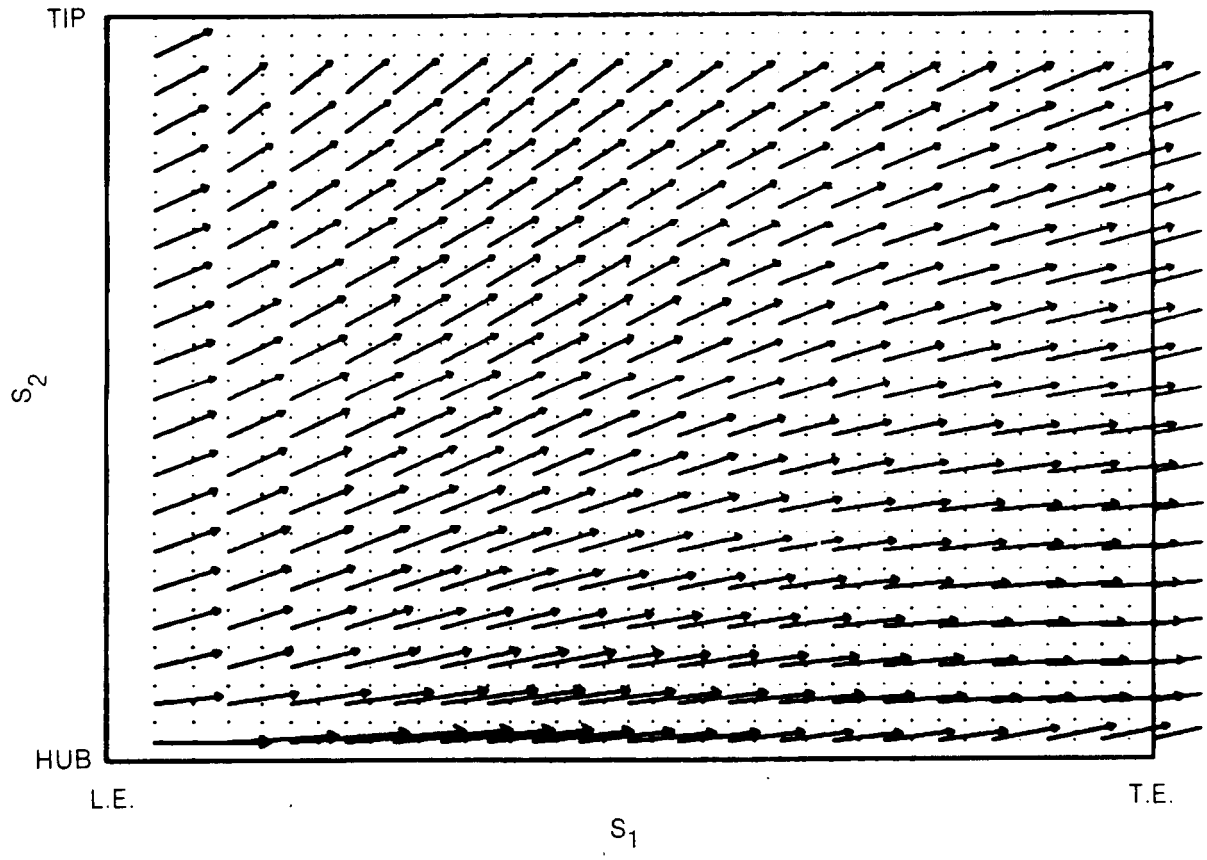

Fig. 22 Boundary Layer Edge Velocity Vectors Calculated from the Experimental Pressure Distribution for the Pressure Surface of a Rotating Turbine Blade

85-1-87-7

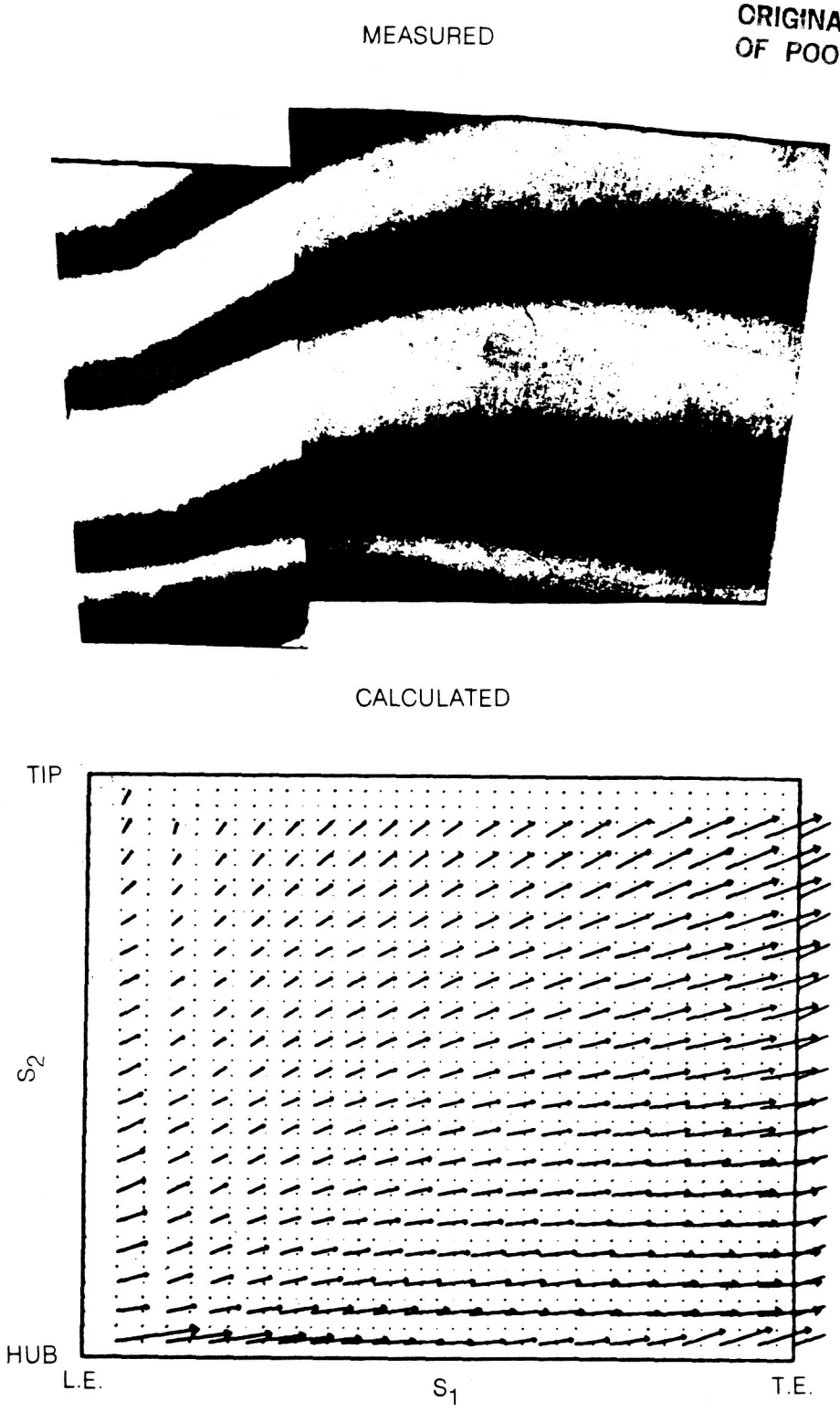

Fig. 23 Measured and Calculated Limiting Streamlines on Pressure Surface of Rotating Turbine Blade

84-12-33-6

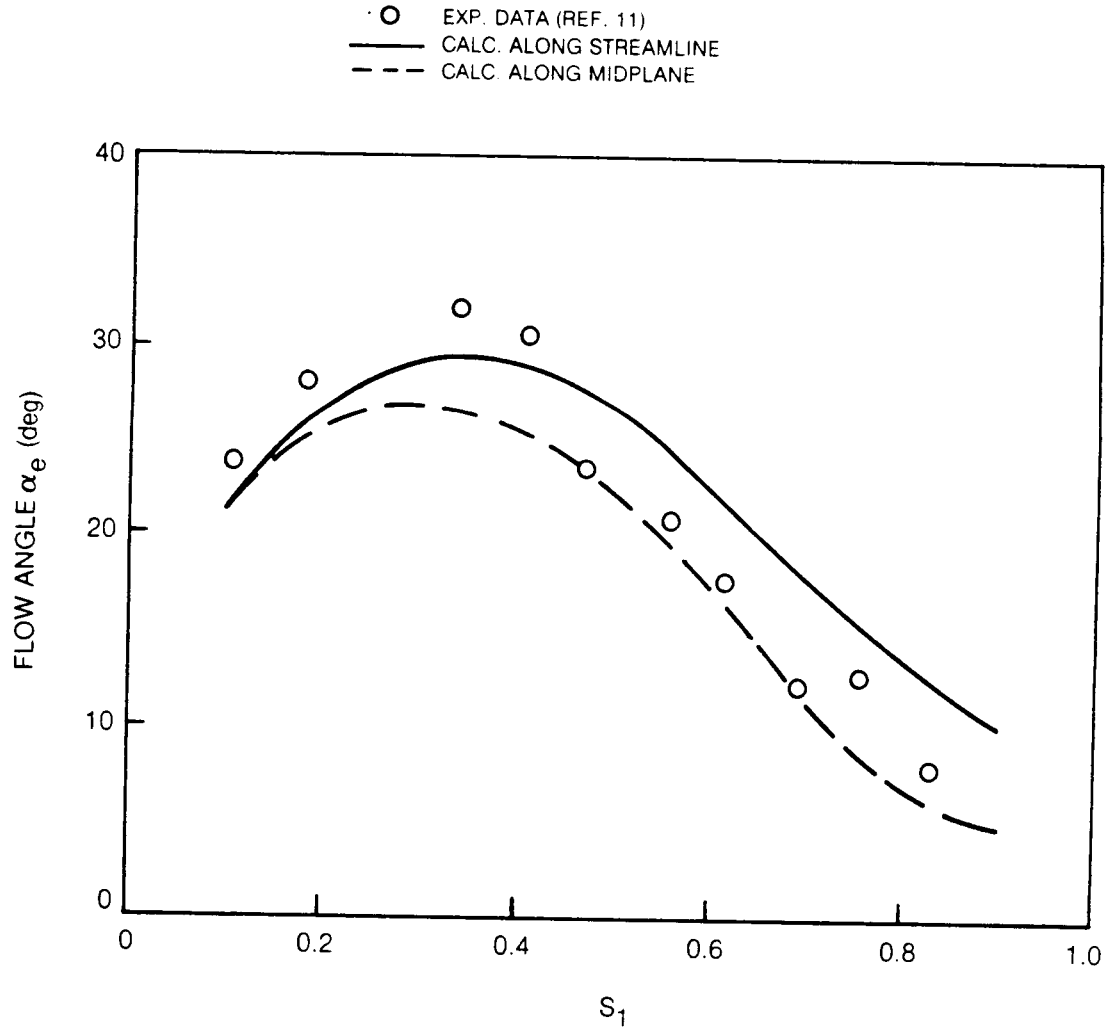

Fig. 24 Calculated and Measured Flow Angle on Pressure Surface of a Rotating Turbine Blade

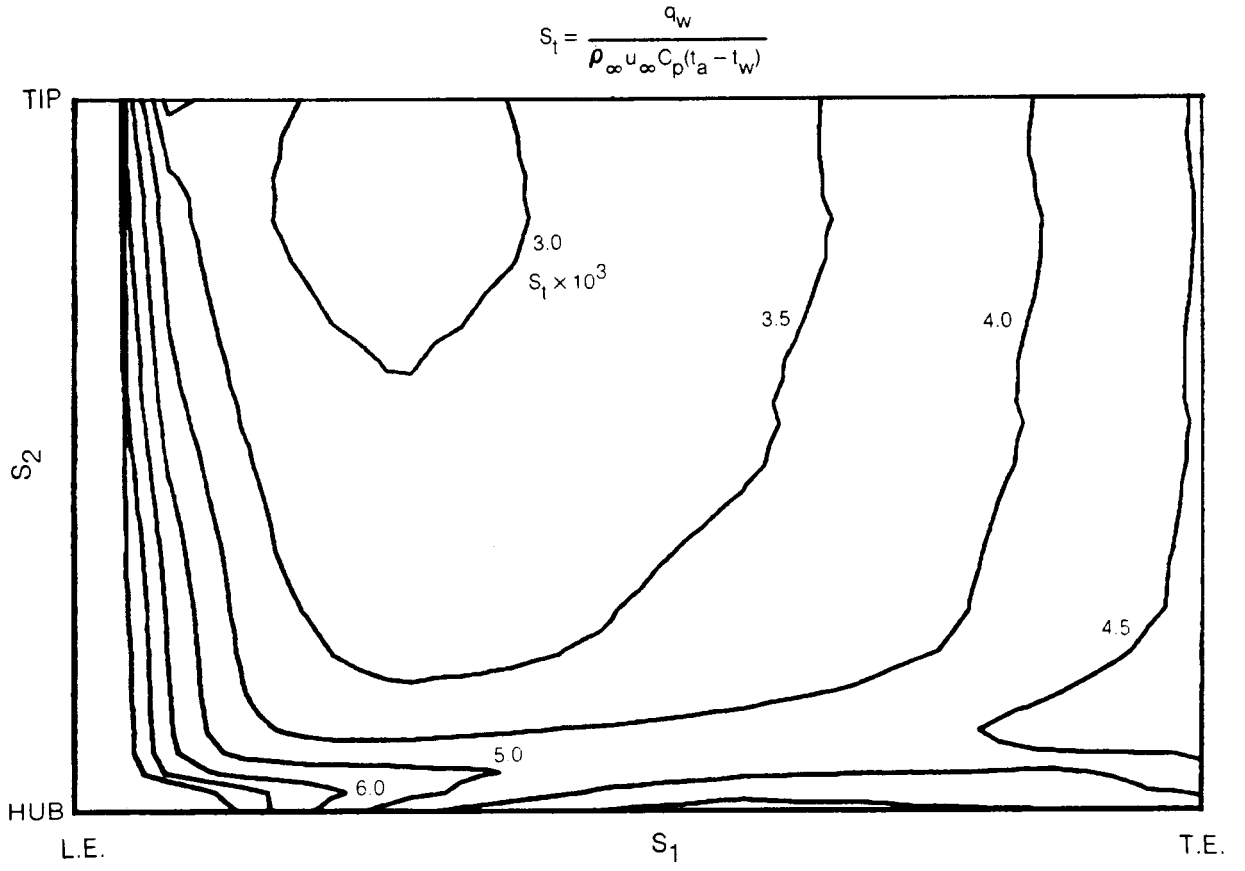

Fig. 25 Calculated Stanton Number Distribution on Pressure Surface of a Rotating Turbine Blade

10.0 APPENDIX - BOUNDARY LAYER PARAMETERS

The boundary layer parameters such as momentum thickness, displacement thickness, and wall shear are calculated in an intrinsic coordinate system (see Ref. 26). This intrinsic coordinate system is oriented with respect to the boundary layer edge flow direction $\vec{U}_e$ and the crossflow direction defined as the $\vec{U}_3 \times \vec{U}_e$ direction. These directions are labeled the streamwise and crossflow direction respectively. The resolution of vectors in this coordinate system is given in Ref. 26 and the following boundary layer parameters are defined.

Displacement Thickness

$$\delta_s^*/\ell = \int \left[1 - \frac{\rho U_s}{\rho_e U_e} \right] dY_3 \tag{A.1}$$

$$\delta_c^*/\ell = \int \left[\frac{\rho U_c}{\rho_e U_e} \right] dY_3 \tag{A.2}$$

Momentum Thickness

$$\theta_{ss}/\ell = \int \frac{\rho U_s}{\rho_e U_e} \left[1 - \frac{U_s}{U_e} \right] dY_3 \tag{A.3}$$

$$\theta_{cc}/\ell = -\int \frac{\rho U_s}{\rho U_c} \frac{U_c}{U_e} dY_3 \tag{A.4}$$

Wall Friction Coefficient

$$C_{fs} = 2\, \tau_{sw}/(\rho_e U_e^2) \tag{A.5}$$

$$C_{fc} = 2\, \tau_{cw}/(\rho_e U_e^2) \tag{A.6}$$

Stanton Number

$$S_t = \frac{\dot{q}_w}{\rho_\infty U_\infty C_p (t_a - t_w)} \tag{A.7}$$

1. Report No. CR174894	2. Government Accession No.	3. Recipient's Catalog No.
4. Title and Subtitle ASSESSMENT OF A 3-D BOUNDARY LAYER ANALYSIS TO PREDICT HEAT TRANSFER AND FLOW FIELD IN A TURBINE PASSAGE		5. Report Date August 29, 1985 6. Performing Organization Code
7. Author(s) O. L. Anderson		8. Performing Organization Report No. R85-956834 10. Work Unit No.
9. Performing Organization Name and Address UNITED TECHNOLOGIES RESEARCH CENTER East Hartford, CT 06108		11. Contract or Grant No. NAS3-23716 13. Type of Report and Period Covered Contractor Report
12. Sponsoring Agency Name and Address NATIONAL AERONAUTICS AND SPACE ADMINISTRATION Washington, DC 20546		14. Sponsoring Agency Code 533-04-12

15. Supplementary Notes

Final Analysis Report - Project Manager, Frederick C. Yeh, Internal Fluid Mechanics Division, NASA Lewis Research Center, Cleveland, Ohio 44135

16. Abstract

An assessment has been made of the applicability of a three dimensional boundare layer analysis to the calculation of heat transfer, total pressure losses, and streamline flow patterns on the surfaces of both stationary and rotating turbine passages. In support of this effort, and analysis has been developed to calculate a general nonorthogonal surface coordinate system for arbitrary three dimensional surfaces and also to calculate the boundary layer edge conditions for compressible flow using the surface Euler equations and experimental pressure distributions. Using available experimental data to calibrate the method, calculations are presented for the pressure, endwall, and suction surfaces of a stationary cascade and for the pressure surface of a rotating turbine blade. The results strongly indicate that the three dimensional boundary layer analysis can give good predictions of the flow field, loss, and heat transfer on the pressure, suction, and endwall surface of a gas turbine passage.

17. Key Words (Suggested by Author(s))	18. Distribution Statement
Boundary Layer Heat Transfer	

19. Security Classif. (of this report)	20. Security Classif. (of this page)	21. No. of Pages	22. Price*
U	U	90	

* For sale by the National Technical Information Service, Springfield Virginia 22151

NASA-C-168 (Rev. 10-75)